Acta Pharmaceutica Sinica B 2024;14(1):223−240

Chinese Pharmaceutical Association
Institute of Materia Medica, Chinese Academy of Medical Sciences

Acta Pharmaceutica Sinica B

www.elsevier.com/locate/apsb
www.sciencedirect.com

ORIGINAL ARTICLE

A multidimensional platform of patient-derived tumors identifies drug susceptibilities for clinical lenvatinib resistance

Lei Sun[a,b], Arabella H. Wan[a,*], Shijia Yan[b], Ruonian Liu[b], Jiarui Li[b], Zhuolong Zhou[c], Ruirui Wu[b], Dongshi Chen[d], Xianzhang Bu[b], Jingxing Ou[e,f], Kai Li[g], Xiongbin Lu[c,h], Guohui Wan[b,*], Zunfu Ke[a,*]

[a]*Department of Pathology, the First Affiliated Hospital, Sun Yat-sen University, Guangzhou 510080, China*
[b]*National-Local Joint Engineering Laboratory of Druggability and New Drug Evaluation, National Engineering Research Center for New Drug and Druggability (Cultivation), Guangdong Province Key Laboratory of New Drug Design and Evaluation, School of Pharmaceutical Sciences, Sun Yat-sen University, Guangzhou 510006, China*
[c]*Department of Medical and Molecular Genetics, Indiana University School of Medicine, Indianapolis, IN 46202, USA*
[d]*Department of Medicine, Keck School of Medicine, University of Southern California, Los Angeles, CA 90033, USA*
[e]*Department of Hepatic Surgery and Liver Transplantation Center, Third Affiliated Hospital, Organ Transplantation Institute, Sun Yat-sen University, Organ Transplantation Research Center of Guangdong Province, Guangdong Province Engineering Laboratory for Transplantation Medicine, Guangzhou 510630, China*
[f]*Guangdong Provincial Key Laboratory of Liver Disease Research, Guangzhou 510630, China*
[g]*Department of Ultrasound, Third Affiliated Hospital, Sun Yat-sen University, Guangzhou 510630, China*
[h]*Melvin and Bren Simon Comprehensive Cancer Center, Indiana University, Indianapolis, IN 46202, USA*

Received 28 June 2023; received in revised form 7 September 2023; accepted 13 September 2023

KEY WORDS

Lenvatinib;
Drug resistance;
High-throughput screening;
Drug discovery;
Patient-derived model;

Abstract Lenvatinib, a second-generation multi-receptor tyrosine kinase inhibitor approved by the FDA for first-line treatment of advanced liver cancer, facing limitations due to drug resistance. Here, we applied a multidimensional, high-throughput screening platform comprising patient-derived resistant liver tumor cells (PDCs), organoids (PDOs), and xenografts (PDXs) to identify drug susceptibilities for conquering lenvatinib resistance in clinically relevant settings. Expansion and passaging of PDCs and PDOs from resistant patient liver tumors retained functional fidelity to lenvatinib treatment, expediting drug repurposing screens. Pharmacological screening identified romidepsin, YM155, apitolisib,

*Corresponding authors.
E-mail addresses: wanguoh@mail.sysu.edu.cn (Guohui Wan), kezunfu@mail.sysu.edu.cn (Zunfu Ke), elliehwann@gmail.com (Arabella H. Wan).
Peer review under the responsibility of Chinese Pharmaceutical Association and Institute of Materia Medica, Chinese Academy of Medical Sciences.

https://doi.org/10.1016/j.apsb.2023.09.015

Romidepsin;
EGFR;
Liver cancer

NVP-TAE684 and dasatinib as potential antitumor agents in lenvatinib-resistant PDC and PDO models. Notably, romidepsin treatment enhanced antitumor response in syngeneic mouse models by triggering immunogenic tumor cell death and blocking the EGFR signaling pathway. A combination of romidepsin and immunotherapy achieved robust and synergistic antitumor effects against lenvatinib resistance in humanized immunocompetent PDX models. Collectively, our findings suggest that patient-derived liver cancer models effectively recapitulate lenvatinib resistance observed in clinical settings and expedite drug discovery for advanced liver cancer, providing a feasible multidimensional platform for personalized medicine.

1. Introduction

Liver cancer accounts for the sixth most common type of human cancer and the fourth-leading cause of cancer-related death worldwide[1]. Liver cancer almost invariably occurs in patients with chronic liver diseases caused by hepatitis B or C virus infection, aflatoxin intake, alcohol abuse, metabolic syndrome, diabetes and obesity. The disease progresses through a ferocious cycle of liver injury, inflammation, regeneration, fibrosis and cirrhosis over decades[2]. Genetic landscape analysis indicates liver cancer's heterogeneity, with frequent mutations in the *TERT* promoter, *TP53*, the genes regulating the WNT pathway and MAPK pathway[3,4]. For the early stage of liver cancer, surgery, liver transplantation, transarterial chemoembolization and radiofrequency ablation may obtain curative potential, while for the advanced stage, systemic targeted therapy and immunotherapy are the only available options but show low efficacy and modest survival benefits[5]. Clinical drug resistance remains as a major obstacle to the treatment of advanced liver cancer and leads to the recurrence of the disease.

Lenvatinib is a second-generation multi-kinase inhibitor that was approved by the FDA in 2017 as the first-line oral therapy for advanced and unresectable liver cancer[6]. Compared to sorafenib, lenvatinib inhibits additional FGFR1-4 mediated signal pathways beyond VEGFR1-3, PDGFR-a/b, RET and KIT[7]. Lenvatinib was proved to be non-inferior to sorafenib treatment regarding overall survival in unresectable liver cancer[8]. However, clinical resistance to lenvatinib treatment eventually developed within 1 or 2 years due to EGFR activation[9] and NF1 loss[10]. Recent attempts by the combination of lenvatinib and pembrolizumab, an anti-PD-1 immune checkpoint inhibitor, obtained superior overall survival in the phase 1b clinical trial and are now in phase III trials[11,12]. Adachi et al.[13] showed that treatment with lenvatinib restored the IFN-γ signaling pathway by inhibiting FGFRs and enhanced the effects of immunotherapy in liver cancer, while Torrens et al.[14] proved that lenvatinib improved the immunomodulatory effects through reducing infiltration of Treg cells and inhibiting the TGF signaling pathway. However, the overall response rate for lenvatinib plus pembrolizumab was only 36% by RECIST v1.1[8], highlighting the urgency of finding more combination therapies that improve the clinical efficacy of lenvatinib-based treatment for liver cancer.

Patient-derived models have recently emerged as a powerful tool for the development of effective personalized therapies in preclinical research. Traditional two-dimensional (2D) culture cancer cell lines have long been used for high-throughput screens for antitumor drugs, but this approach lacks clinical relevance and fails to provide phenotypic and genetic heterogeneity in the primary tumors[15,16], and thus has low success rate in translating investigational antitumor drugs to the clinic[17]. Recent liver cancer cell repository was established to interrogate the pharmacogenomics landscape with unexplored gene-drug associations, offering an opportunity for drug discovery in liver cancer[18]. Patient-derived organoids (PDO) were generated to model the tumor microenvironment with primary tissue architecture and function[19–23]. In a recent study, we reported tumor-organoid models with tumor-specific cytotoxic T cells for evaluating the epigenetic inhibitors that enhance antigen presentation and T-cell-mediated cytotoxicity[24], highlighting the essential role of PDO in validation of screened drugs. However, examples of patient-derived models directly from patients with drug resistance remain sparse, and limited evidence is now available to predict effective treatments for patients with advanced liver cancer in the clinic.

In this study, we describe a multidimensional and high-throughput platform for drug screening in advanced liver cancer, in which patient-derived models are built upon clinical tissue samples with lenvatinib resistance. Drug candidates identified in the PDC model were validated in the PDO and PDX models for overcoming lenvatinib resistance in liver cancer. A unique mouse xenograft model with a patient-autologous immune system was developed to predict the effectiveness of the drug candidate for lenvatinib-based combination therapy in the pre-clinic. The PDC-PDO-PDX standardized and unbiased platform established in this study can be used to facilitate the rapid identification of drug susceptibility for lenvatinib-resistant liver cancer.

2. Materials and methods

2.1. Tissue and cell culture

The lenvatinib-resistant liver tumors were acquired from Sun Yat-sen University the Third Affiliated Hospital and were reviewed and approved by the institutional review board. This study followed all related legal and ethical regulations for research involving human subjects. Human liver cancer cell lines HepG2, Huh7, SNU449, MHCC97H, MHCC97L, PLC/PRF/5 and mouse liver cancer cell line Hepa1-6 and H22 were acquired from American Type Culture Collection. Cell lines were kept in multiple backups after receiving to decrease the chance of phenotypic drift and detected mycoplasma contamination by Mycoplasma Stain Assay Kit (C0296, Beyotime, China). The authentication of cell lines was verified by the STR analysis by GenePrint10 System

(B9510, Promega, USA). Cell culture conditions were 37 °C in 5% CO_2, and the working medium used Dulbecco's modified Eagle's medium (Corning, USA) with 10% FBS.

2.2. Generation of patient-derived tumor organoids and cell lines

Tumor-derived organoids were extracted and incubated primarily as previous reports[24,25], and modified as demonstrated. Briefly, tumor tissues from patient or PDX tumor-derived specimens (~0.25−1 cm^3) were fragmented and cultured at 37 °C with the digestion solution (Collagenase I 1 mg/mL; Hyaluronidase 0.1 mg/mL; DNase I 0.1 mg/mL). Tumor tissues were incubated for 30 min to 1 h depending on digestion conditions. Specifically, digestion was terminated by FBS until no fragments of tissue were observed, and subsequently the cultured suspension was filtered by a nylon cell strainer (100 μm) and centrifuged at 300−400 × *g* for 5 min. Single cell suspensions were first seeded with a high density and distributed to a lower density after ~1 week. The expanding organoids were passed with a dilution ratio of 1:2−1:3 every 2−3 weeks by advanced medium DMEM/F12 (GIBCO) plus 1% glutamax, 1% penicillin/streptomycin, 1.25 mmol/L *N*-acetyl-L-cysteine, 10 mmol/L HEPES, 50 ng/mL recombinant human EGF, 100 ng/mL recombinant human FGF7, 100 ng/mL recombinant human FGF10, 25 ng/mL recombinant human HGF, 3 nmol/L dexamethasone and 10 μmol/L Y27632. A gelatin-coated cell culture dish was used to promote the adhesion of organoid-derived tumor cells to generate PDCs. Fibroblasts were removed using a Miltenyi Biotec Tumor-Associated Fibroblast Isolation Kit (#130-116-474, Miltenyi Biotec, Germany). The initial passages of organoids and PDCs were stocked and frozen with 10% DMSO and 90% FBS in liquid nitrogen.

2.3. PDC-PDO viability assay

For PDC viability assay, as described previously[26], PDCs were tested to evaluate their susceptibility to various drugs (Topscience) and combination with lenvatinib or sorafenib. Cells were counted and seeded into 96-well plates with 2000 cells per well and cultured for 24 h. A library of 80 drugs (1 μmol/L) and the combination (1 μmol/L library compound + 10 μmol/L sorafenib, 1 μmol/L library compound + 10 μmol/L lenvatinib) were added to the cells with the indicated concentrations and cultured for 72 h. Cell proliferation after treatment was examined by Cell Counting Kit-8 (C0037, Beyotime, China) using a microplate reader (ThermoFisher, USA).

For PDO viability assay, inoculate 200 μL PDO spheres into non-adherent 96-well plates and treat with romidepsin, YM155, apitolisib, NVP-TAE684, dasatinib, lenvatinib, and sorafenib at concentrations of 0, 0.625, 1.25, 2.5, 5, and 10 μmol/L for 72 h. The 96-well plate was placed under a microscope for photography. Then, the PDO spheres were mixed thoroughly and 100 μL was taken for quantitative analysis by CellTiter-Glo® 3D Cell Viability Assay (G9681, Promega, USA). The CellTiter-Glo® 3D Reagent was thawed at room temperature. And 100 μL of PDO spheres were added to each well of a white opaque 96-well plate and then an equal amount of assay reagent was added to each well. Finally, the 96-well plate was placed on a shaker to mix the contents vigorously for 5 min to induce cell lysis. After 30 min of incubation and stabilization, the luminescent signal at room temperature, the luminescence was recorded by GloMax® Navigator (GM2000, Promega, USA).

For PDO IHC assay, 3 mL PDO spheres were inoculated into non-adherent 6-well plates and romidepsin at concentrations of 2.5, 5, and 10 μmol/L was added and incubated for 24 h. PDO spheres were collected and treated with romidepsin by centrifuging at 1000 rpm for 5 min, the supernatant was discarded, and 1 mL of polyformaldehyde solution was added for preservation in preparation for IHC experiments.

2.4. Dendritic-cell-based phagocytosis

Monocyte-derived dendritic cells were isolated from peripheral blood monocytes with $CD14^+$ population by magnetic beads (130-050-201, Miltenyi Biotec, Germany). Cells were differentiated by culturing with IL-4 and GM-CSF using CellXVivo Human Monocyte-derived DC Differentiation Kit (CDK004, R&D, USA) and harvested on Day 6. PDCs were treated with romidepsin for 24 h at indicated concentrations and stained with 5 μmol/L CFSE (565082, BD Biosciences, USA), and subsequently co-cultured with moDCs at 1:1 ratio for 12 h. MoDCs were stained by CD11B antibodies labeled with PE (101207, Biolegend, China) for surface marking. Immunofluorescence figures were taken by a fluorescence microscope (Nikon, Japan).

2.5. ATP level detection assay

The ATP level in cells was detected by the ATP Assay Kit (S0026, Beyotime, China) followed by the manufacturer's instruction. The protein amounts from supernatant samples were measured by the BCA protein assay kit (P0011, Beyotime, China) to normalize the ATP level per microgram protein.

2.6. HMGB1 release assay

PDC cells were treated with romidepsin at indicated concentrations, and the level of released HMGB1 in the supernatant was measured after 24 h by the HMGB1 ELISA Kit (ST51011, IBL International, Germany).

2.7. Flow cytometry

Flow cytometry analysis of PDOs was performed after two-week of PDO cultures by using APC anti-human CD45 (304011), FITC anti-human CD31 (303103), PE anti-human CD140a (323505) and FITC anti-human EpCAM (369813) antibodies from Biolegend (Guangzhou, China). Flow cytometry analysis of PDCs was performed after romidepsin administration for 24 h. Cells were collected and divided into 1 × 10^6 cells/100 μL in FACS tubes. Fc receptors were blocked with IgG (1 μg IgG/10^6 cells) at room temperature for 15 min. The cells were mixed with conjugated primary antibody CRT (h/m/r Calreticulin A7, R&D, USA, IC38981N-100UG, 5−10 μL/10^6 cells), and incubated at room temperature in darkness for half an hour. The cells were subsequently washed with 2 mL flow cytometry staining buffer (FC001, R&D, USA) to remove any unbound antibodies. For quantitative analysis, cells were then resuspended with 400 μL flow cytometry staining buffer and loaded in flow cytometry (BD Biosciences, USA).

2.8. Immunohistochemistry

Formalin-fixed paraffin-embedded tumor and organoid samples were cut with 5 μm thick on polarized glass. The endogenous

peroxidase activity and non-specific staining were blocked before sections incubating with primary antibodies against Ki67 (ab15580, Abcam, USA), caspase-3 (ab32351, Abcam, USA) and CD8 (C8/144B, Abcam, USA) at 4 °C overnight. Immunohistochemistry analysis was stained with horseradish peroxidase conjugates by using DAB detection, while nuclei were counterstained with Hoechst. The stained sections were pictured with Nikon microscope (Japan).

2.9. Animal experiments

All procedures for animal experiments were testified and performed compliant with the regulations of the Institutional Animal Care and Use Committee of Sun Yat-sen University (SYSU-IACUC-2020-B1041). For subcutaneous implantation mouse models, 60 BALB/c-*nu*/*nu* mice (6-week-old) were divided into three groups randomly and implanted 5×10^5 PDC-P0, and 5×10^5 HepG2, 5×10^5 SNU499, 5×10^5 PLC/PRF/5, 5×10^5 Huh7, 5×10^5 MHCC97L cells respectively. 32 BALB/c-*nu*/*nu* mice (6-week-old) were implanted 5×10^5 PDC-P0 or 5×10^5 PDC-P10 cells were then divided into four groups randomly and treated with corn oil, sorafenib (50 mg/kg, T0093L, Topscience, China), lenvatinib (4 mg/kg, T0520, Topscience, China) and romidepsin (2 mg/kg, T6006, Topscience, China) respectively by intraperitoneal injection every two days. 28 (or 24) wild-type C57BL/6 mice (6-week-old) were implanted 5×10^5 Hepa1-6 or H22 cells and were randomly divided into four groups treated with corn oil, romidepsin (2 mg/kg), anti-PD1 antibody (200 μg), and romidepsin (2 mg/kg) plus anti-PD1 antibody (200 μg, BE0146, BioXCell, USA) respectively, romidepsin treated by intraperitoneal injection every two days and anti-PD1 antibody treated by intraperitoneal injection every three days.

For the PDX mouse model, lenvatinib-resistant liver tumor tissues were acquired from Sun Yat-sen University the Third Affiliated Hospital and the experiments were testified by the institutional review board. Lenvatinib-resistant liver cancer tissues were subcutaneously implanted into BALB/c-*nu*/*nu* mice to establish the PDX mouse model. All mice were separated into four groups randomly when the tumor size was measured to 100 mm^3, and subsequently injected with corn oil, sorafenib (50 mg/kg), lenvatinib (4 mg/kg) and romidepsin (2 mg/kg) respectively by intraperitoneal injection every two days.

For the humanized PDX model, 32 NOD/SCID/IL2r$\gamma^{-/-}$ (NSG) mice (6-week-old) were separated into four groups randomly. Cyclophosphamide (150 mg/kg in saline) and disulfiram (125 mg/kg in 0.8% Tween-80 in saline) were prepared before the experiments. All mice were intraperitoneally injected with cyclophosphamide and oral administrated with disulfiram once per day for 2 days. Oral administration of disulfiram was administered for 2 h after each dose of cyclophosphamide. Venous blood was drawn from an autologous patient. PBMCs were extracted and purified by Ficoll−Paque (GE Healthcare) density gradient centrifugation according to the manufacture's protocol. One day after the second-round treatment of cyclophosphamide and disulfiram, 2.5×10^6 PDC cells and 5×10^6 purified PBMCs that mixed with phosphate-buffered saline and 50% Matrigel in a 200 μL volume were subcutaneously injected in the right flank of mice. Four groups were treated with corn oil, sorafenib (50 mg/kg), lenvatinib (4 mg/kg) and romidepsin (2 mg/kg), respectively, by intraperitoneal injection every two days when tumor size reached about 100 mm^3. Tumors were recorded by a caliper every 2 days to measure tumor growth. When tumors became necrotic or their volume reached over 1000 mm^3, mice were sacrificed. At the treatment endpoint, tumor xenografts were collected and fixed with 4% PFA for paraffin-embedded section analysis and immunohistochemistry analysis.

2.10. RNA extraction and quantitative RT-PCR analysis

Total RNAs were isolated by Trizol (Invitrogen, USA) according to the manufacturer's protocol. Complementary DNAs were synthesized by using the SuperScript™ III First-Strand Synthesis System DNA (18080051, ThermoFisher, USA). RT-PCR was performed by SYBR-Green Master Mix (RR820B, Takara, Japan) in 7500 apparatus (ABI, USA). The primers used in this study were listed in Supporting Information Table S1.

2.11. Whole-exome sequencing analysis

PDC cells were sent for whole-genome sequencing (WGS). The raw sequencing data were submitted to the SRA database (PRJNA946708). After the original sequenced reads were obtained, the information analysis process was performed with the human reference genome. Low-quality reads (<Q20) were deleted by trimming of the ends of the reads. Cutadapt was used to remove sequencing adaptors. Sequencing alignment was performed by using Bowtie2 (v2.2.6) to the UCSC hg38 genome reference, and the output results were preprocessed by Picard (v1.113) for variant calling *via* labeling duplicates, and InDel realignments were conducted by the GATK toolkit (v3.7). Detect variation information in samples, and statistically and annotate the detected variation.

2.12. RNA sequencing and data analysis

TRIzol (15596018, Thermo, USA) was used to isolate and purify RNA according to the manufacturer's protocol. The quantity and purity of the total RNA were assessed using NanoDrop (Thermo, USA), and the integrity of the RNA was checked by Bioanalyzer 2100 (Agilent, USA), with concentration >50 ng/μL, RIN value > 7.0, and total RNA > 1 μg meeting downstream experimental requirements. Oligo (dT) magnetic beads (25-61005, Thermo, USA) were used for specific capture of mRNA with PolyA tails through two rounds of purification. The captured mRNA was fragmented using a NEBNextR Magnesium RNA Fragmentation Module kit (NEBNextR Magnesium RNA Fragmentation Module (E6150S, NEB, USA) at 94 °C for 5−7 min. The fragmented RNA was performed PCR amplification with sequencing adapters, resulting in a library with a fragment size of 300 bp ± 50 bp (strand-specific library). Finally, the library was sequenced using Illumina NovaseqTM 6000 (LC Bio Technology Co., Ltd., Hangzhou, China) in paired-end mode with PE150 sequencing.

The reads obtained from sequencing machines contain raw reads that may include adapters or low-quality bases, which can negatively impact subsequent assembly and analysis. Therefore, in order to obtain high-quality, clean reads, the reads were filtered further using Cutadapt (version: cutadapt-1.9). We then aligned reads of all samples to the reference genome (hg38) by HISAT2 (version: hisat2-2.2.1). The reads that were mapped for each sample were assembled using StringTie (version: stringtie-2.1.6) with default parameters. Subsequently, all transcriptomes from the various samples were merged to reconstruct a comprehensive

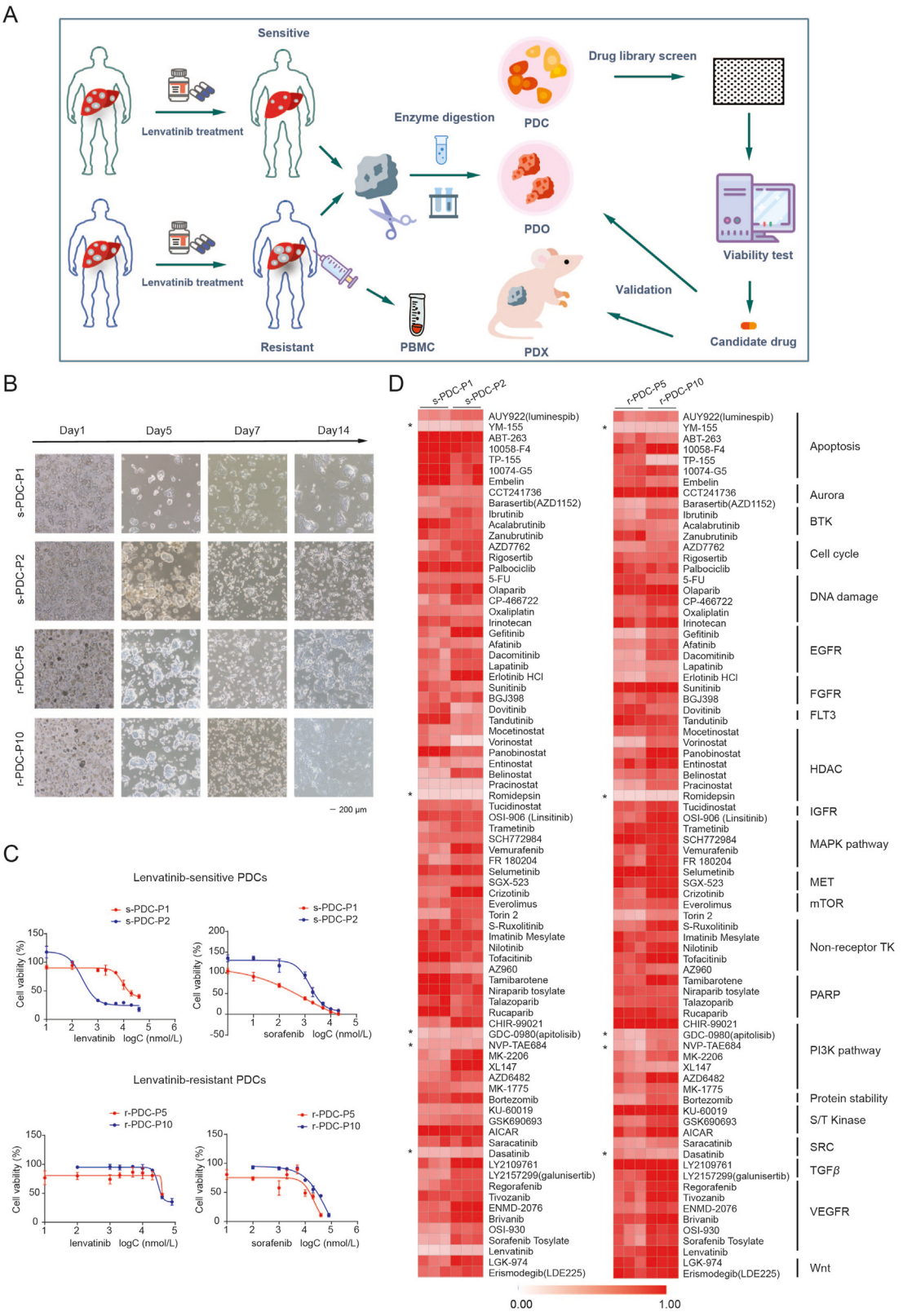

Figure 1 Drug sensitivity in PDCs from patients with lenvatinib resistance. (A) Schematic approach of *ex vivo* expansion of liver cancer PDCs, PDOs and PDXs from patients with clinical lenvatinib resistance and drug sensitivity quantification by PDCs-based screening. (B) Cell growth and morphological changes of lenvatinib-sensitive PDCs (s-PDCs) and lenvatinib-resistant PDCs (r-PDCs) with indicated expansion of culture time. (C) Cell viability of patient-derived cell lines with clinical lenvatinib sensitivity or resistance in response to lenvatinib or sorafenib treatment at various doses. (D) Heatmaps representing cell viability of lenvatinib-sensitive and lenvatinib-resistant PDCs treated with a library of targeted agents. Normalization by DMSO treatment. In all relevant panels, $*P < 0.05$, two-tailed *t*-test. Data are presented as mean ± SD ($n = 3$).

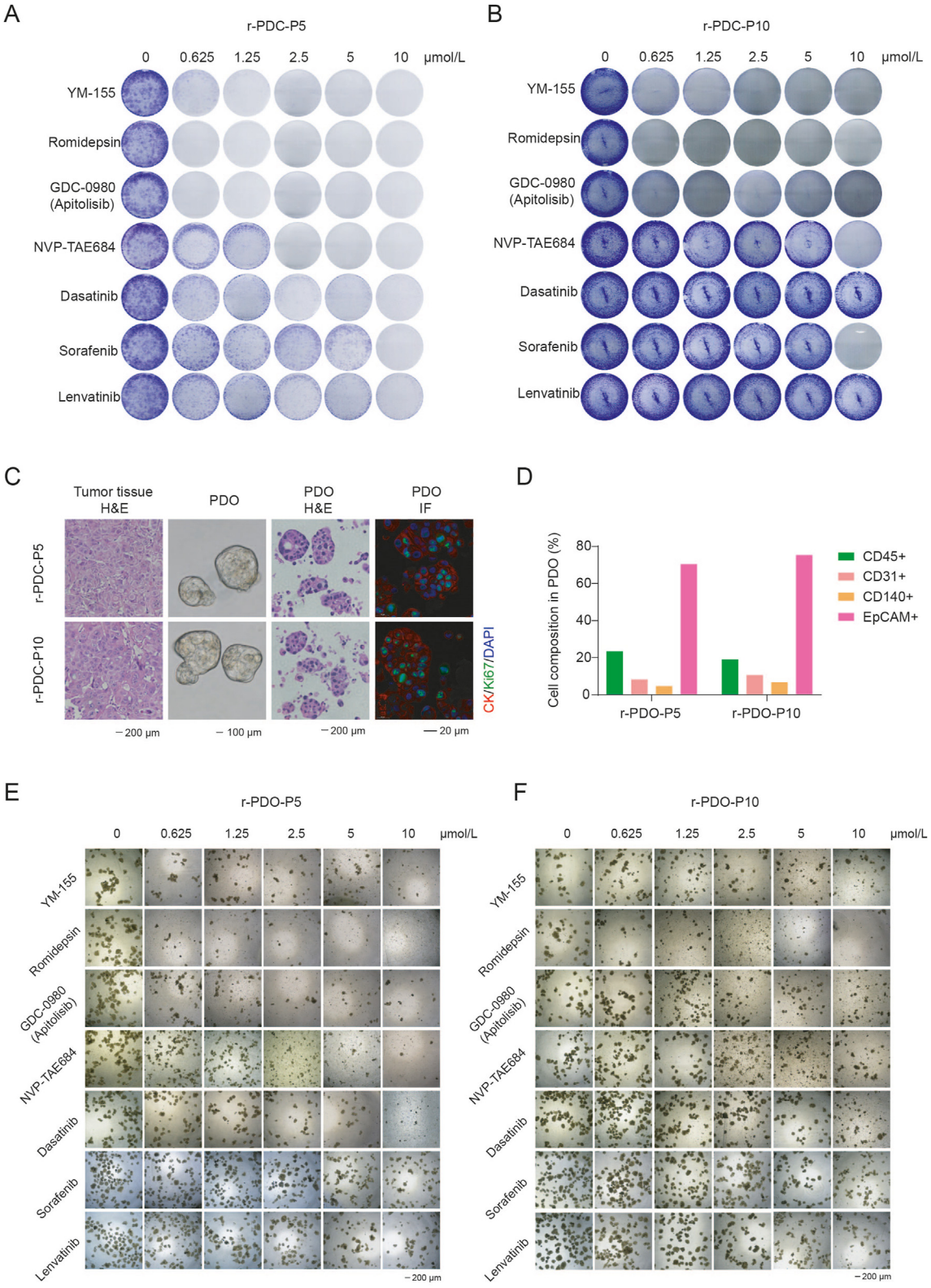

Figure 2 Validation of representative drugs for clinical lenvatinib resistance in liver cancer PDCs and PDOs. (A, B) Long-term colony-formation assay of lenvatinib-resistant PDC-P5 cell line (A) and PDC-P10 cell line (B) treated with representative drugs, YM-155, romidepsin, GDC-0980, NVP-TAE684 and dasatinib. Lenvatinib and sorafenib were used as controls. (C) Representative images of non-adherent organoids culture. From top to bottom, H&E staining on liver tumors from resistant Patient 5 and Patient 10; morphology of PDO spheroids; H&E staining of PDOs; immunofluorescent staining of PDOs with cytokeratin (CK, red), Ki67 (green), and DAPI (blue). (D) The cellular composition of PDOs with indicated antibodies analyzed by flow cytometry analysis. (E, F) Representation of selected screen hits in lenvatinib-resistant r-PDO-P5 (E) and r-PDO-P10 (F). YM-155, romidepsin, GDC-0980, NVP-TAE684 and dasatinib were selected to treat patient-derived organoids at various concentrations. Sorafenib and lenvatinib were used as controls.

transcriptome using gffcompare software (version: gffcompare-0.9.8). Once the final transcriptome was generated, StringTie and ballgown were utilized to estimate the expression levels of all transcripts and perform expression abundance for mRNAs by calculating FPKM (fragments per kilobase of transcript per million). Differential expression analysis of genes was conducted using DESeq2 software. Genes exhibiting a false discovery rate (FDR) parameter below 0.05 and an absolute fold change of ≥ 2 were considered differentially expressed. These genes were subsequently subjected to enrichment analysis of GO functions and KEGG pathways. The raw sequencing data has been submitted to the GEO database (GSE227751).

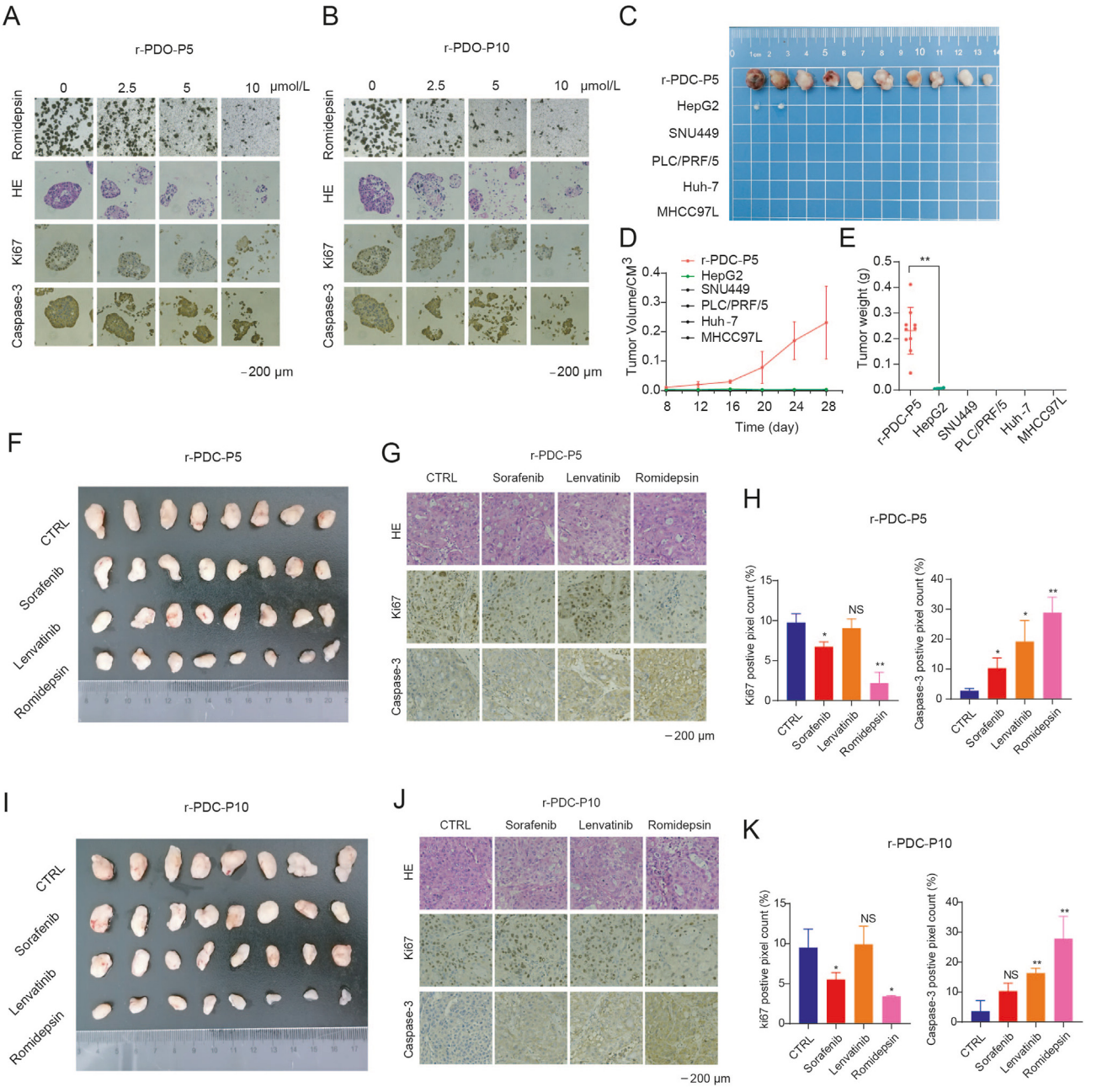

Figure 3 Romidepsin is an effective drug susceptibility for lenvatinib-resistant PDCs and PDOs. (A, B) Representative images of non-adherent patient-derived organoids r-PDO-P5 (A) and r-PDO-P10 (B) treated with romidepsin, respectively. H&E staining, immunohistochemistry of Ki67 and caspase-3 were measured in r-PDO-P5 and r-PDO-P10. (C−E) Growth of patient-derived cell line and other human liver cell lines *in vivo* (C). 5×10^5 r-PDC-P5, SNU449, MHCC97H, PLC/PRF/5 and Huh7 cells were subcutaneously injected in nude mice, respectively. Tumor growth curves (D) and tumor weights (E) of these cell line xenografts. (F−K) Tumor images of r-PDC-P5 (F) and r-PDC-P10 (I) xenografts after treatment with sorafenib, lenvatinib and romidepsin, respectively. H & E staining, immunohistochemistry of Ki67 and caspase-3 in r-PDC-P5 (G) and r-PDC-P10 (J) -derived xenografts treated with sorafenib, lenvatinib and romidepsin, respectively. Quantification of Ki67 and caspase-3 expression in IHC images from r-PDC-P5 (H) and r-PDC-P10 (K) was analyzed by Image Pro Plus (IPP) analysis, respectively. In all relevant panels, $^*P < 0.05$; $^{**}P < 0.01$; ns, no significant; two-tailed *t*-test. Data are presented as mean ± SD ($n = 3$).

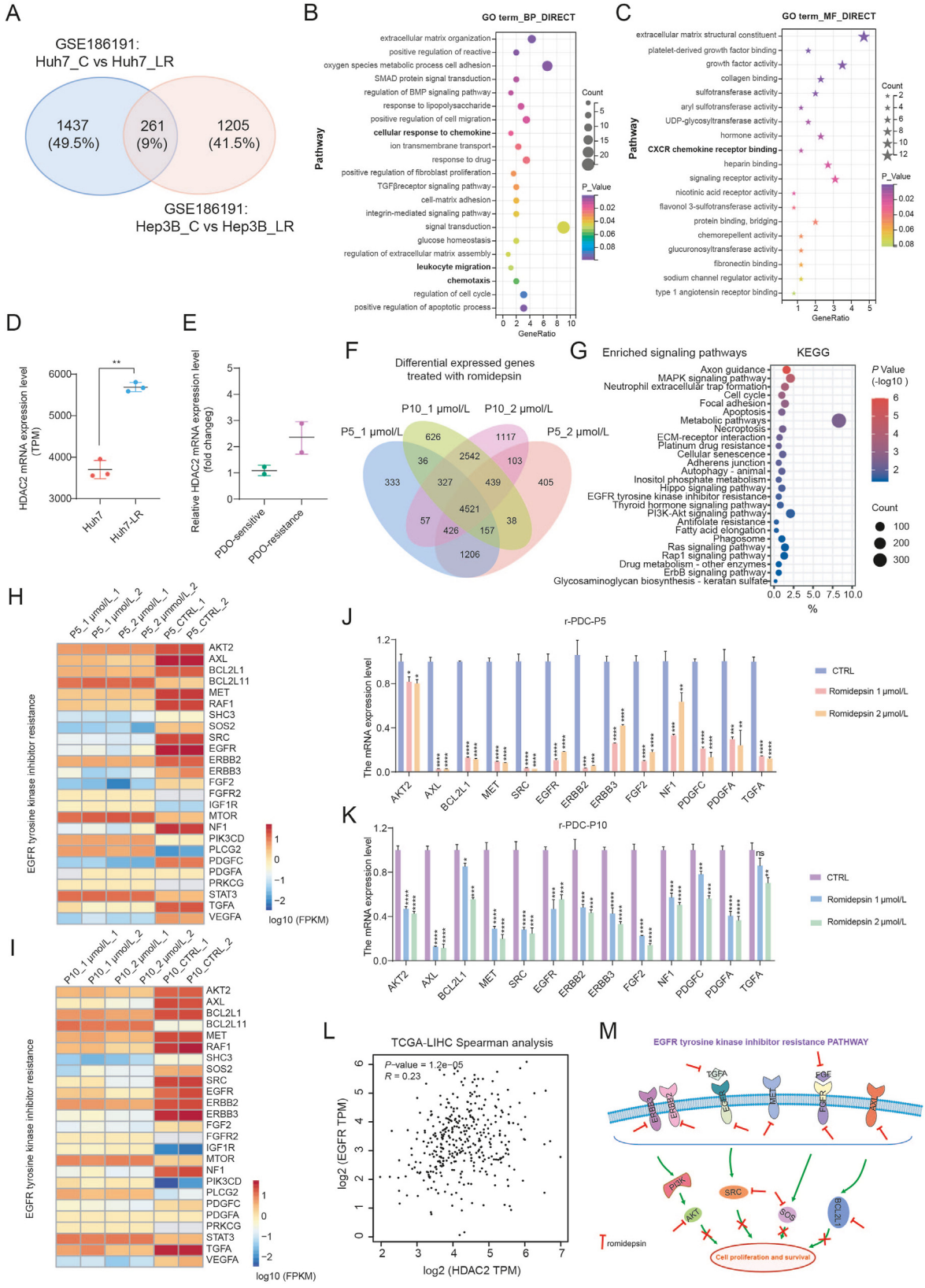

Figure 4 Romidepsin blocks activation of EGFR tyrosine kinase signaling pathway in lenvatinib-resistant liver cancer. (A) Overlap of differentially expression genes (DEGs) associated with lenvatinib resistance in Huh7 and Hep3B cells (GSE186191). C, control; LR, lenvatinib resistance. (B, C) Functional annotation of altered genes associated with lenvatinib resistance from through Gene Ontology (GO) analysis of biological process (BP) (B) and molecular function (MF) (C) analysis. (D) HDAC2 RNA expression levels in lenvatinib resistant Huh7 cells. (E) HDAC2 RNA expression levels in lenvatinib-sensitive PDOs and lenvatinib-resistant PDOs by qRT-PCR assay. (F) Overlap of differentially

2.13. Statistics analysis

All the experiments were carried out at least 3 times and a representative experiment was given. Means and standard deviation (SD) were used and analyzed by using GraphPad prism 8.0. The statistical difference between indicated groups was analyzed and compared by two-tailed Student's *t*-test. Statistical significance was accepted for *P*-values of <0.05. *P* values are shown and indicated on plots in means of follows ($^{*}P < 0.05$, $^{**}P < 0.01$; $^{***}P < 0.001$, $^{****}P < 0.0001$).

3. Results

3.1. Large-scale screen of drug sensitivity in lenvatinib-resistant PDCs in vitro

To establish a high-throughput drug screening platform for lenvatinib-based liver cancer therapy, we generated patient-derived cell lines and organoids directly from patient specimens. Liver tumor tissues (~1 cm^3) from patients with clinical lenvatinib resistance or lenvatinib sensitivity were surgically removed and divided into three parts for further generation of primary cell line (PDC), organoid (PDO) and xenograft (PDX) models, respectively (Fig. 1A). As fresh clinical specimens provide insufficient cell quantities for large-scale drug screens, primary cell lines and organoids needed *ex vivo* expansion before viability testing with potential drug libraries (Fig. 1A). We optimized the PDC culture protocol by promoting PDO adhesion instead of direct single-cell suspension culture from dissociated patient tumor tissues, resulting in improved success rate and reduced culture time to 2 weeks (Fig. 1B).

To evaluate the clinical resistance of TKIs in liver cancer, we first verified the drug resistance of prevalent human liver cancer cell lines to lenvatinib and sorafenib. HepG2 and Huh7 cells showed sensitivity upon increasing concentrations of lenvatinib and sorafenib, whereas other cell lines demonstrated intrinsic resistance in long-term clonogenic assays (Supporting Information Fig. S1A and S1B). Next, we confirmed the clinical TKI treatment response in our established PDC cell lines. After 72 h of lenvatinib treatment, IC_{50} values were 425.1 ± 137.1 nmol/L in s-PDC-P1 cells, and 152.2 ± 63.8 nmol/L in s-PDC-P2 cells. As expected, r-PDC-P5 and r-PDC-P10 cells showed significantly higher viability ($IC_{50} > 30$ μmol/L), indicating severe lenvatinib resistance. Similarly, 72-h sorafenib IC_{50} values were 26.2 ± 0.5 μmol/L in s-PDC-P1 cells and 990 ± 312 nmol/L in s-PDC-P2 cells, while r-PDC-P5 and r-PDC-P10 cells also showed severe sorafenib resistance ($IC_{50} > 20$ μmol/L) (Fig. 1C). These results indicate that PDC expansion and passaging directly from patient liver tumors retained functional fidelity towards lenvatinib treatment.

To identify effective therapeutic strategies against clinical lenvatinib resistance, we performed sensitivity tests on lenvatinib-sensitive and lenvatinib-resistant PDCs using a drug panel of 80 compounds (Supporting Information Table S2) that consist of a range of essential regulators in cell growth and cell survival, including growth factors, signal pathways, apoptosis modulators, protein regulators, DNA damage sensors and tyrosine kinases. These compounds were previously tested for bypass tracks and several additional clinical targets[27]. In this scenario, lenvatinib-sensitive and lenvatinib-resistant PDCs were tested against the panel with or without lenvatinib or sorafenib (Fig. 1D, Fig. S1C and Supporting Information Table S3). Notably, YM-155 (survivin inhibitor), romidepsin (histone deacetylase inhibitor), GDC-0980/apitolisib (PI3K inhibitor), NVP-TAE684 (ALK inhibitor) and dasatinib (tyrosine kinase inhibitor) exhibited significant activity in both lenvatinib-sensitive and lenvatinib-resistant liver cancer PDC cells regardless of lenvatinib or sorafenib presence, suggesting these five compounds as monotherapies in these 2D tumor cell models.

To characterize the genomic landscape of lenvatinib-resistant PDCs, we performed whole-genome sequencing (WGS) analysis to examine somatic alterations in r-PDC cell lines. We identified 3,405,711 single nucleotide polymorphisms (SNPs) in r-PDC-P5 cell line and 3,410,545 SNPs in r-PDC-P10 cell line, with a moderate difference in InDel length distribution (Supporting Information Fig. S2A and S2B). Deletion (DEL) and inter-chromosomal translocation (CTX) were the predominant events in our lenvatinib-resistant PDC cell lines, and a distinct copy of number of variation (CNV) was observed on the X chromosome in r-PDC-P5 cell line (Fig. S2C and S2D). Consistent with the known genomic landscape of liver cancer[25,26], we identified deletion of *TP53*, *NRAS* and duplication of *PIK3CA*, *MYC* in both two r-PDC cell lines. Notably, we detected deletions and mutations in *FGFR1*, *EGFR*, *BRAF*, *TGFBR3*, *PDGFRA*, *IGF1R* and *RAF1*, indicating potential mechanisms of lenvatinib clinical resistance in liver cancer (Fig. S2E). Furthermore, we found duplications of *ROS1* and *HDAC2* as undescribed events in lenvatinib resistance, illustrating the potential for the present treatment scheme to discover patient-specific effective combination therapy.

3.2. Validation of representative drug candidates in lenvatinib-resistant PDCs and PDOs

To validate the screened drug candidates, we first employed clonogenic assays to assess long-term effects on lenvatinib resistance

expressed genes (DEGs) in r-PDC-P5 and r-PDC-P10 cells treated with romidepsin at various doses. (G) KEGG pathway enrichment analysis of DEGs treated with romidepsin. (H, I) Romidepsin treatment impaired the EGFR tyrosine kinase inhibitor resistance pathway in lenvatinib-resistant PDCs. Heatmap showed mRNA expression level changes in genes associated with multiple tyrosine kinase pathways after romidepsin treatment in r-PDC-P5 (H) and r-PDC-P10 (I) cells. (J, K) Validation of gene expression levels related to the EGFR tyrosine kinase inhibitor resistance pathway in r-PDC-P5 (J) and r-PDC-P10 (K) cells with romidepsin treatment by qRT-PCR. (L) Correlation between HDAC2 and EGFR in the TCGA-LIHC database by Spearman's analysis. (M) The schematic diagram illustrates the primary molecular mechanisms involved in inhibiting the EGFR tyrosine kinase inhibitor resistance pathway following romidepsin treatment. Romidepsin exhibits a multi-target inhibitory effect that reverses lenvatinib-resistant signaling pathways. This includes suppressing the expression of related receptors (EGFR, ERBB2, ERBB3, FGFR, MET, and AXL), growth factors (TGFA and FGF), and downstream effectors (AKT, SRC, SOS, and BCL2L1). EGFR, epidermal growth factor receptor; ERBB2/3, Erb-B2 receptor tyrosine kinase 2/3; FGFR, fibroblast growth factor receptor; MET, proto-oncogene, receptor tyrosine kinase; AXL, AXL receptor tyrosine kinase; TGFA, transforming growth factor alpha; FGF, fibroblast growth factor; AKT, AKT serine/threonine kinase; SRC, the SRC proto-oncogene, non-receptor tyrosine kinase; SOS, SOS ras/rac guanine nucleotide exchange factor; BCL2L1, BCL2 like 1, an apoptosis regulator. In all relevant panels, $^{*}P < 0.05$; $^{**}P < 0.01$; ns, no significant; two-tailed *t*-test. Data are presented as mean ± SD ($n = 3$).

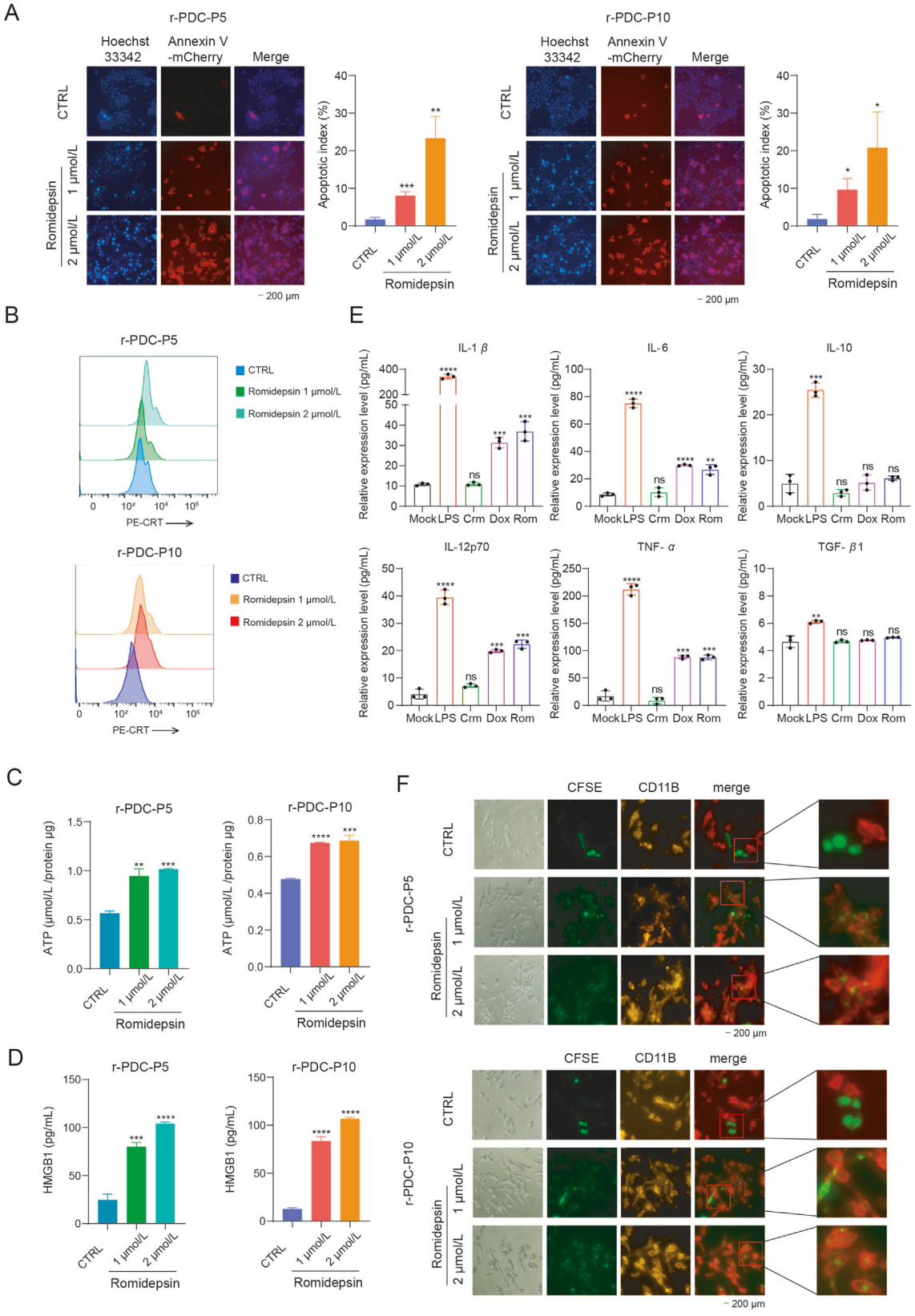

Figure 5 Romidepsin triggers immunogenic cell death in liver cancer resistant PDCs *in vitro*. (A) Romidepsin induced apoptosis in lenvatinib-resistant liver cancer r-PDC-P5 and r-PDC-P10 cells. Quantification of apoptotic cells was analyzed by IPP. (B) Romidepsin induced calreticulin (CRT) expression in lenvatinib-resistant liver cancer r-PDC-P5 and r-PDC-P10 cells by flow cytometry analysis. (C) Romidepsin induced ATP production in lenvatinib-resistant liver cancer r-PDC-P5 and r-PDC-P10 cells. (D) Romidepsin induced HMGB1 protein level in lenvatinib-resistant liver cancer r-PDC-P5 and r-PDC-P10 cells by ELISA assays. (E) Romidepsin-treated PDCs stimulated dendritic cells to release

in PDC models. Only YM-155, romidepsin and GDC-0980/apitolisib showed consistent antitumor activity in both r-PDC-P5 and r-PDC-P10 cells, while resistance emerged against NVP-TAE684 and dasatinib in r-PDC-P10 cells (Fig. 2A and B). Next, we established lenvatinib-resistant patient-derived organoids to verify these representative drug candidates in a 3D semisolid extracellular matrix. Histological analysis showed notable morphological similarities shared among PDOs and original biopsies tumor tissues. After one week of *in vitro* culture, PDOs formed dense spheres with various gland-like phenotypes and stained positive for pan-cytokeratin and Ki67, indicating liver tumor cells (Fig. 2C). The cellular composition of resistant PDOs indicated that tumor cells (positive for $EpCAM^+$) constituted the majority (~70%) compared to other cell types, including immune cells (positive for $CD45^+$), vascular endothelial cells (positive for $CD31^+$) and tumor-associated fibroblasts ($CD140^+$) (Fig. 2D). Upon treatment with drug candidates, romidepsin exerted the most promising antitumor activity in both r-PDO-P5 and r-PDO-P10 3D tumor models at does as low as 0.625 μmol/L (Fig. 2E and F). YM-155, GDC-0980/apitolisib, NVP-TAE684 and dasatinib showed more potent antitumor effects in r-PDO-P5 than those in r-PDO-P10, suggesting potential distinct clinical responses. Collectively, we developed a sequential PDC-PDO platform to expedite the identification of efficacious compounds targeting clinical lenvatinib resistance.

3.3. *Romidepsin is a potent drug for liver cancer with lenvatinib resistance in vivo*

Romidepsin, also known as Istodax, is a histone deacetylase (HDAC) inhibitor initially approved by the FDA in 2009 for treatment of cutaneous T cell lymphoma (CTCL) in patients with systemic therapy. Prior research regarding romidepsin as a treatment for lenvatinib-resistant liver cancer is scarce[28]. However, our screening platform tested pharmacological interrogation with clinical samples, uncovering the functional relevance of histone acetylation and uncharacterized genetic variants in lenvatinib resistance. Interestingly, among eight testing HDAC inhibitors, only romidepsin displayed potent antitumor activity in liver cancer. Romidepsin exhibits the highest sensitivity towards HDAC1 and HDAC2 among these inhibitors, which may account for its superior inhibitory effect at the cellular level (Supporting Information Fig. S3A). Romidepsin treatment significantly reduced organoid growth in sensitive PDO groups, displaying similar effects to sorafenib and lenvatinib treatments (Fig. S3B and S3C). Importantly, romidepsin treatment showed remarkable antitumor activity in resistant PDO models in a dose-dependent manner, as indicated by the downregulation of Ki67 and upregulation of caspase-3 (Fig. 3A and B).

To further evaluate romidepsin's efficacy *in vivo*, we first examined the tumorigenicity of resistant PDC cell lines by subcutaneously injecting 5×10^5 r-PDC cells into nude mice, using HepG2, SNU449, PLC/PRF/5, Huh7 and MHCC97L cells as controls. While conventional human liver cell lines struggled to form subcutaneous tumors in nude mice, our r-PDC cells displayed enhanced *in vivo* tumorigenic capabilities, as indicated by increased tumor size and tumor weight (Fig. 3C−E), providing a robust patient-derived cell line model for liver cancer *in vivo* study. Administering romidepsin to these PDC-derived xenografts in immune-deficient mice resulted in elevated sensitivity to romidepsin treatment in both r-PDC-P5- and r-PDC-P10-derived xenografts compared to sorafenib or lenvatinib treatments, as shown by decreased tumor sizes and tumor weights (Fig. 3F, I, and Supporting Information Fig. S4A−S4D). Histopathological analysis showed that romidepsin treatment, which restored histone acetylation, significantly suppressed Ki67 expression and induced caspase-3 expression in lenvatinib-resistant tumor tissues (Fig. 3G−H, J−K). To further assess the pharmacological effects of romidepsin on tumor heterogeneity, we tested romidepsin treatment in the primary resistant PDX mouse model. Invariably, romidepsin treatment substantially suppressed growth and weight of r-PDX-P1 tumors compared to the control group, although sorafenib or lenvatinib treatments also mildly decreased tumor growth in r-PDX models (Fig. S4E−G). To evaluate and compare the antitumor efficacy of romidepsin with other HDAC inhibitors, we first measured the expression levels of HDAC1 and HDAC2 in Huh-7 cells treated with 8 HDAC inhibitors including vorinostat, panobbinostat, entinostat, belinostat, pracinostat, romidepsin, tucidinostat and mocetinostat (Supporting Information Fig. S5A). HDAC1 was significantly downregulated while HDAC2 was slightly downregulated in Huh-7 cells upon treatment with panobbinostat and romidepsin, respectively. Additionally, we employed a syngeneic mouse model in which Hepa1-6 cells were subcutaneously injected into C57BL/6 mice. Among the eight HDAC inhibitors administered, romidepsin exhibited the most potent inhibitory activity, while the other HDAC inhibitors also demonstrated a degree of tumor reduction *in vivo* (Fig. S5B−S5D). These results suggest that romidepsin may serve as a second-line treatment for lenvatinib-resistant liver cancer.

3.4. *Romidepsin blocks EGFR signaling pathway in liver cancer PDCs*

Romidepsin displayed the most potent antitumor activity in our lenvatinib-resistant PDCs, prompting an investigation into the underlying mechanism of how romidepsin conquers lenvatinib resistance in liver cancer. We first analyzed RNA-seq data for parental and lenvatinib-resistant liver cancer cells (GSE186191) (Fig. 4A−C) and found HDAC2 expression upregulated in lenvatinib-resistant Huh7 cells, consistent with results from two sensitive and two resistant PDOs (Fig. 4D and E). To examine romidepsin's effects, transcriptome sequencing was performed on r-PDCs treated with two doses of romidepsin (1 and 2 μmol/L). Overall, 4521 significantly changed genes were analyzed and overlapped in these two r-PDC cells (Fig. 3F). Kyoto Encyclopedia of Genes and Genomes (KEGG) pathway analysis indicated romidepsin treatment activated signaling pathways mediating platinum drug resistance, antifolate resistance and EGFR tyrosine kinase inhibitor resistance (Fig. 3G, Fig. S5A and S5B). Notably, romidepsin dramatically decreased the expression of genes involved in multiple tyrosine kinase pathways, including AKT2,

cytokines *in vitro*. Positive control doxorubicin (Dox) or negative control C2 ceramide (Crm) were used, respectively. (F) Romidepsin stimulated dendritic cell-mediated phagocytosis in lenvatinib-resistant liver cancer r-PDC-P5 and r-PDC-P10 cells. CSFE (green) signal labeled PDC cells; CD11B (red) signal labeled DCs. In all relevant panels, $*P < 0.05$; $**P < 0.01$; $***P < 0.001$; $****P < 0.0001$; ns, no significant; two-tailed *t*-test. Data are presented as mean ± SD ($n = 3$).

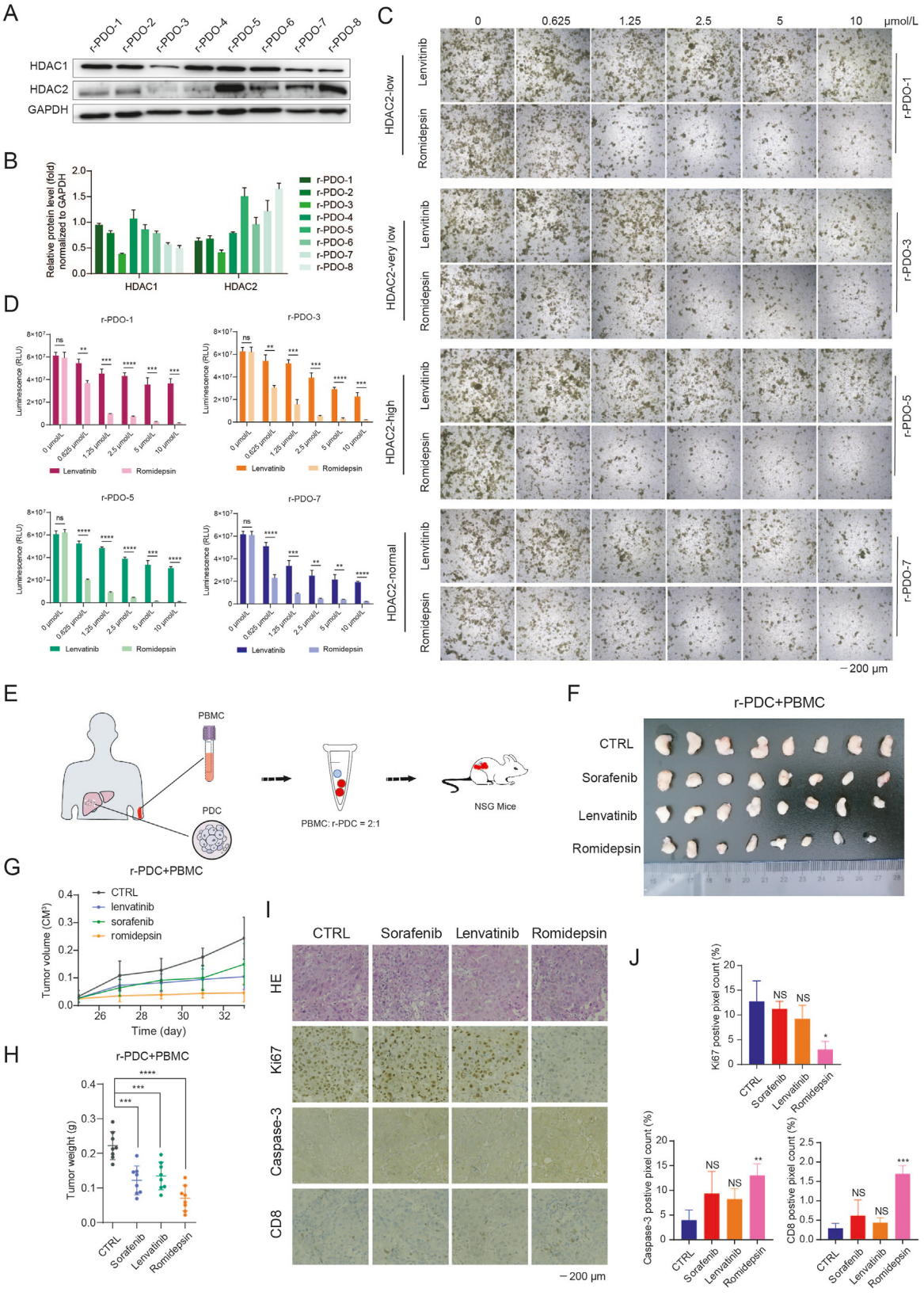

Figure 6 Response of romidepsin-therapy in lenvatinib-resistant PDOs and humanized immune system mouse model. (A) Expression of HDAC1 and HDAC2 in 8 HCC patients with lenvatinib-resistance. The protein levels were measured in cultured-PDOs by Western blot. (B) Quantification of HDAC1 and HDAC2 expression in r-PDOs by Image J analysis. (C) Representation of selected images in lenvatinib-resistant PDOs after treatment with various concentrations of lenvatinib and romidepsin. (D) The fluorescence intensity of r-PDO-1, r-PDO-3, r-PDO-5 and r-PDO-7 were detected after different concentrations of lenvatinib and romidepsin treatment using CellTiter-Glo® 3D Reagent. (E) Schematic

MET, RAF1, SRC, EGFR, ERBB3, TGFA and VEGFA, indicating complementary and synergistic effects with romidepsin blockage in lenvatinib resistance (Fig. 4H and I). We further validated gene expression levels related to cell proliferation and survival in both r-PDC-P5 and r-PDC-P10 cells. Specifically, romidepsin inhibited EGFR, ERBB2/3, MET, FGER and AXL signaling pathways, as evidenced by key component reduction in these pathways by qRT-PCR (Fig. 4J and K). Analyzing the TCGA-LIHC database revealed a positive correlation between HDAC2 and EGFR expression (Fig. 4L). We confirmed downregulation of the EGFR, ERBB2/3, MET, FGER and AXL signaling pathways in Huh-7 cells with HDAC-2 depletion (Supporting Information Fig. S6C). Collectively, these results indicate that romidepsin treatment effectively blocks the EGFR signaling pathway to conquer lenvatinib resistance in liver cancer (Fig. 4M).

3.5. *Romidepsin triggers immunogenic cell death in liver cancer PDCs*

Interestingly, we noticed a correlation between lenvatinib resistance and leukocyte migration and chemotaxis factors, suggesting potential immunotherapy implications (Fig. 4B and C). We also noticed that romidepsin caused neutrophil extracellular trap formation, ECM-receptor interaction and autoimmune thyroid disease pathways, hinting at the activation of immunity-related signals in these two r-PDC models (Fig. 4G and Fig. S6D). Previous studies have reported romidepsin enhancing immunogenicity of tumor cells, thereby improving clinical efficacy[29,30]. In this scenario, we analyzed romidepsin's ability to induce immune cell response in resistant liver cancer cells. Romidepsin treatment induced apoptosis in lenvatinib-resistant r-PDC-P5 and r-PDC-P10 cells in a concentration-dependent manner, as indicated by increased Annexin V levels (Fig. 5A). To determine whether romidepsin-mediated apoptosis could cause immunogenic cell death (ICD), a form of apoptosis that induces an effective immune response toward tumor cells by activation of dendritic cells and consequent initiation of T cell-mediated immune response[31], we examined the release of ICD characteristic damage-associated molecular patterns (DAMPs) in r-PDC cells treated with romidepsin. Our results revealed significant induction of DAMPs, including calreticulin (CRT), high-mobility-groups box 1 (HMGB1) and adenosine triphosphate (ATP) in r-PDC-P5 and r-PDC-P10 cells, suggesting potential ICD activation upon romidepsin treatment (Fig. 5B−D). To examine maturation of patient's peripheral blood monocyte cell (PBMC)-derived dendritic cells, we measured cytokines, including IL-1β, IL-6, IL-10, IL-12, TNFα, and TGFβ, secreted by dendritic cells. Dendritic cells were cocultured for 24 h with r-PDC cells pre-treated with DMSO (mock), C2 ceramide (Crm, a negative control), doxorubicin (Dox, a positive control) and romidepsin (Rom). As expected, Dox- or Rom-treated r-PDC cells stimulated dendritic cells to secrete cytokines such as IL-1β, IL-6, IL-12 and TNFα but not IL-10 or TGFβ *in vitro*. As a negative control, Crm-treated r-PDC cells failed to stimulate dendritic cells to secrete any of the above cytokines (Fig. 5E). As CRT functions as an "eat me" signaling marker for dendritic cells[31], we assessed dendritic cells with phagocytosis of romidepsin-mediated apoptotic liver cancer cells. Our results showed a dramatically enhanced phagocytosis of tumor cells by dendritic cells in the romidepsin-treated group by compared with the control group, as indicated by the increase of carboxyfluorescein succinimidyl ester (CFSE)-stained r-PDC cells within CD11B-stained dendritic cells *via* fluorescence microscopy (Fig. 5F). These data indicate that romidepsin may function as an ICD inducer in lenvatinib-resistant liver cancer cells.

To assess *in vivo* efficacy of romidepsin as an immuno-oncology agent, we examined its effect in two syngeneic mouse models using murine liver cancer cell line Hepa1-6 and H22, implanted into wild-type C57BL/6 mice with functional immunity. We measured the sensitivity of Hepa1-6 and H22 cells to romidepsin and lenvatinib treatments, finding both drugs exhibited antitumor effects *in vitro* (Supporting Information Fig. S7A and S7B). Consistently, romidepsin administration effectively suppressed liver cancer growth *in vivo*, as shown by reduced tumor size and tumor weight (Fig. S7C−S7H). Given the immunogenic cell death observed for romidepsin, we determined whether it could trigger an efficient antitumor immune response *in vivo*, and the combination of romidepsin and immune checkpoint blockade could enhance antitumor effects in liver cancer. In the syngeneic mouse models, while PD-1 blockade and romidepsin treatment moderately suppressed Hepa1-6 and H22 cell growth, combination therapy led to an 85% and 60% reduction in size and weight of Hepa1-6-derived tumors, and an 85% and 85% reduction in size and weight of H22-derived tumors *in vivo*, respectively (Fig. S7C−S7H). Romidepsin treatment, alone or combined with PD-1 therapy, induced cellular apoptosis and suppressed tumor cell proliferation compared to the control group (Fig. S7H−S7L). Together, these data demonstrate romidepsin's ability to improve the antitumor effects of anti-PD-1 therapy in liver cancer.

3.6. *Response of romidepsin-therapy in lenvatinib-resistant PDOs and humanized immune system mouse model*

As romidepsin specifically inhibits HDAC1 and HDAC2 activity[32], we determined whether varying HDAC1 and HDAC2 levels would influence romidepsin's therapeutic effects in lenvatinib-resistant liver cancer. In this scenario, we validated the response of romidepsin-therapy in 8 additional liver cancer patients with clinical lenvatinib-resistance. HDAC1 showed similar protein expression, while HDAC2 expression was less robust across patients (Fig. 6A and B). Romidepsin treatment achieved maximal inhibitory effects on tumor growth in r-PDOs models with high HDAC2 levels, such as patient #5, while also demonstrated effective retardation of tumor growth in r-PDOs with normal or low levels of HDAC2 (Fig. 6C and D). In addition, we established a timely and cost-effective humanized liver cancer xenograft

diagram of humanized immune system mouse model. Autogenous patient-derived peripheral blood mononuclear cells (PBMCs) and lenvatinib-resistant PDCs (ratio = 2:1) were mixed and xenografted in NSG mice. (F) Tumor images of r-PDC xenografts in humanized immune system mouse models. The r-PDC-derived PDXs were treated with sorafenib, lenvatinib and romidepsin, respectively. (G) Growth curves of r-PDC-derived PDXs in humanized immune system mouse model. (H) Tumor weight of r-PDC-derived PDXs in humanized immune system mouse model. (I) H & E staining, immunohistochemistry of Ki67, caspase-3 and CD8 in r-PDC-derived PDXs treated with sorafenib, lenvatinib and romidepsin, respectively. (J) Quantification of Ki67, caspase-3 and CD8 expression in IHC images by Image Pro Plus (IPP) analysis. In all relevant panels, $*P < 0.05$; $**P < 0.01$; $***P < 0.001$; $****P < 0.0001$; two-tailed *t*-test. Data are presented as mean ± SD ($n = 3$).

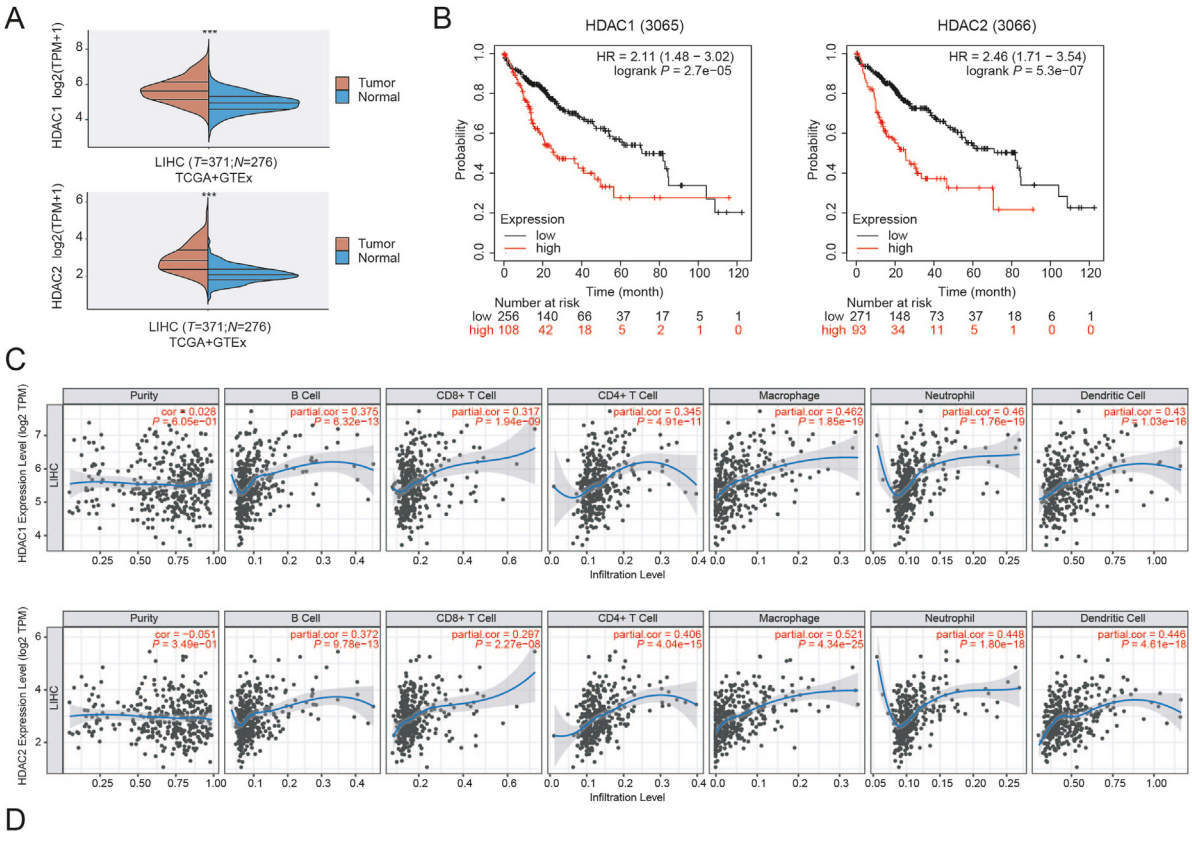

	2D cell culture	Syngeneic model	PDX	Tumor organoids	Multidimensional platform (PDC-PDO-hPDX)
Ease of establishing system	+	+++	++	++	+
High-throughput screening	+++	–	–	+	+++
Cost efficiency	++	+	–	+	++
Time savings	++	+	+	+	+++
Biological stability	+	++	++	++	++
Heterogeneity	–	–	++	+	++
Genetic manipulation	++	++	–	+	++
Preservation of tumor microenviroment	–	++	++	+	++
Preservation of immune system interactions	–	++	–	–	+

Figure 7 Clinical significance of HDAC1 and HDAC2 in liver cancer. (A) Expression levels of HDAC1 and HDAC2 in human liver tumors and normal liver tissues in TCGA and GTEx databases. (B) Clinical significance of HDAC1 and HDAC2 by evaluating low expression and high expression in liver cancer from TCGA database. Significance was determined by a log-rank test. (C) The correlation of HDAC1 and HDAC2 expression with immune infiltration levels in liver cancer in TCGA database. (D) Comparison of multidimensional platform (PDC-PDO-hPDX) with traditional single patient-derived model. Relative advantages and disadvantages for drug effectiveness screening for personalized medicine were summarized with the respective features described as best (+++), suitable (++), possible (+) and unsuitable (−) according to previous reports[37–40].

mouse model by engrafting the same patient's peripheral blood mononuclear cells (PBMCs) and recapitulating human immunity in humanized mice (Fig. 6E). The NOD/SCID/IL2r$\gamma^{-/-}$ (NSG) mice were treated with cyclophosphamide for myeloablation before subcutaneously injection of the mixture of the same patient's PBMCs and r-PDC cells. Liver cancer xenografts with no sign of graft versus host disease (GvHD) on Day 25 were administered with romidepsin, sorafenib and lenvatinib, respectively. Our results show romidepsin exhibited superior antitumor activity *in vivo* in the humanized PBMC-NSG liver cancer xenograft model compared to sorafenib and lenvatinib, as shown by decreased tumor size and tumor weight (Fig. 6F–H). Significant infiltration of human $CD8^+$ T cells was detected in r-PDC-derived tumor tissues in the romidepsin treatment group, along with decreased Ki67 levels and elevated caspase-3 levels (Fig. 6I and J). We detected a slight reduction of tumor size and tumor weight in humanized liver cancer xenograft mice upon treatment with sorafenib and lenvatinib (Fig. 6F–H), however, infiltration of human $CD8^+$ T cells in PDC-derived xenografts was not significantly different in comparison to the control group (Fig. 6I and J).

Next, we performed transcriptomic profiling analysis of liver cancers in TCGA and GTEx databases to investigate the clinical significance of HDAC1 and HDAC2 in human liver cancers. Both HDAC1 and HDAC2 were found to be upregulated in liver cancers (Fig. 7A). The clinical prognostic impact of HDAC1 and HDAC2 showed that higher levels of either were correlated with poorer overall survival in liver cancer patients (Fig. 7B). Interestingly, by examining the correlation of HDAC1 and HDAC2 levels with immune infiltration levels, we found that both HDAC1 and HDAC2 expression levels were highly associated with infiltrated immune cells, including B cell, macrophage, $CD8^+$ T cell, $CD4^+$ T cell, dendritic cells and neutrophils (Fig. 7C). This suggests that HDAC1 and HDAC2 play a role in the orchestration of immune responses to liver cancer development and drug resistance. Collectively, these results demonstrated that romidepsin serves as an effective therapy for lenvatinib resistance in both r-PDO models and humanized immune system mouse models.

4. Discussion

Liver cancer remains one of the most difficult cancers to cure because liver cancer is commonly detected at advanced stages with metastases. Lenvatinib, an oral multi-kinase inhibitor, became the second FDA-approved as a first-line therapy in 2019 for treating advanced unresectable liver cancer, ending sorafenib's decade-long monopoly as the sole systemic therapy[6]. However, clinical drug resistance remains a major obstacle for effective and efficient therapeutic interventions in human cancers[33,34]. Arechederra et al.[35] showed that increased level of a secreted glycoprotein ADAMTSL5 caused induction of several oncogenic inputs involved in drug resistance of multiple receptor tyrosine kinases inhibitors including sorafenib, lenvatinib, and regorafenib. The upregulation of ADAMTSL5 was caused by hyper-methylation of CpG islands at the gene body, which highlights the fact that aberrant epigenetic alterations are involved in drug resistance. Similarly, our previous study also demonstrated that aberrant expression of FOXO3 mediated by abnormal RNA modification caused activation of autophagy and resulted in sorafenib-resistance in liver cancer[36]. Understanding the mechanism of resistance to lenvatinib is essential for developing novel therapeutic avenues in liver cancer. A recent study reported that EGFR activation limited the therapeutic efficacy of liver cancer to lenvatinib[9]. The combination of lenvatinib treatment and EGFR inhibition exhibited lethal effects in patients with EGFR expression while this drug combination displayed less effect in patients with low EGFR, which consist of more than 50% of liver cancer patients. Therefore, identifying novel effective drug susceptibility to combat lenvatinib resistance is urgent to yield good clinical benefits of lenvatinib-based therapies for liver cancer.

Patient-derived models, including PDC, PDO and PDX models, have emerged as compelling tools for cancer research and drug development due to their multidimensional coverage, consistent pedigrees, and close resemblance to clinical responses in therapeutic intervention. Our integrated PDC-PDO-hPDX model offers a time-saving and cost-effective high-throughput screening methods for evaluating drug resistance, compared to traditional primary cell culture, xenograft generation, and tumor organoid formation techniques[37–41] (Fig. 7D). To study lenvatinib resistance in liver cancer, we established patient-derived cell lines from patient specimens with lenvatinib resistance. Our modified culturing technology, based on aligned organoids[24,25], shortened PDC generation time to within 2 weeks, facilitating high-throughput drug screens. Whole genome sequencing (WGS) analysis of r-PDCs identified genomic changes related to lenvatinib resistance, including alterations in FGFR1, EGFR, BRAF, TGFBR3, PDGFRA, IGF1R and RAF1. Jin et al.[9] previously revealed a protective mechanism mediated by the EGFR–PAK2–ERK5 signaling pathway that limited the response of liver cancer to lenvatinib treatment. However, deletion of the EGFR signal pathway was identified in our r-PDC cell lines, indicating an alternative protective mechanism was present for lenvatinib resistance. Notably, the alterations of ROS1 and HDAC2 were identified from WGS analysis. Recurrent ROS1 signaling contributed to the activation of the JAK–STAT pathway in liver cancer[42], and targeting ROS1 could be used to treat patients with high levels of RNase7[43]. HDAC2 serves as a chromatin modifier involved in cell cycle, apoptosis and differentiation in liver cancer, inhibition of HDAC2 was considered as a novel strategy for therapeutic intervention for liver cancer[44,45]. While the genomic analysis provided proof-of-concept for ROS1 or HDAC2 blockage as potential treatment schemes for liver cancer with lenvatinib resistance, we could verify these findings with our standardized multidimensional platform in the clinical setting.

Through a pharmacological screen of potential compounds that could conquer lenvatinib-resistance in liver cancer, we identified YM-155, romidepsin, apitolisib, NVP-TAE684 and dasatinib from our lenvatinib-resistant cell lines and organoids. YM-155 is a survivin inhibitor and displayed potent anti-tumor activity in refractory mantle cell lymphoma with ibrutinib and venetoclax resistance[46]. Apitolisib is a dual PI3K and mTOR inhibitor, and was reasonably tolerated at high dose (30 mg) in pleural mesothelioma patients with modest and durable antitumor effects[47], but was less effective than everolimus in patients with metastatic renal cell carcinoma[48]. NVP-TAE684 is a potent ALK inhibitor and was used to overcome docetaxel or pemetrexed resistance in non-small lung cancer with rearranged ALK[49]. Dasatinib is an oral dual inhibitor of BCR/ABL and Src subfamily tyrosine kinase and was reported to display highly synergistic effects in combination therapy with trametinib in patients with diffuse intrinsic pontine glioma[50]. Romidepsin has confirmed activity as a potent and selective inhibitor of HDAC1 and HDAC2 and was shown to resensitize acute myeloid leukemia to chemotherapy by

eradicating leukemia stem cell marker (CD123) positive cells[51]. Previous studies have shown some pan-histone deacetylase inhibitors including resminnostat, CKD-5 and entinostat displayed synergistic effects on TKI-sensitive liver cancer cells[52–55]. Based on the WGS analysis from our patient-derived lenvatinib-resistant cells, HDAC2 was altered with duplication during the formation of lenvatinib resistance and romidepsin exhibited the most potent antitumor activity in both PDC and PDO models. However, our later validation experiments of romidepsin treatment in additional resistant PDO models indicated that romidepsin displayed consistent robust antitumor effects towards lenvatinib resistance regardless of HDAC2 status. Romidepsin has been reported to target class I and II HDAC enzymes. Previous studies have shown that romidepsin exhibits high affinity for HDAC1, HDAC2, and HDAC3, which are class I HDAC enzymes[32]. Additionally, it demonstrates affinity for class II HDAC enzymes (HDAC4, HDAC5, HDAC6, HDAC7, HDAC8 and HDAC9), though with slightly higher IC_{50} values compared to those for class I HDACs[56,57]. Besides the multiple HDAC targets inhibited by romidepsin, alternative mechanisms involved in lenvatinib resistance in liver cancer have been reported in some studies[58]. These studies identified two key resistance genes, neurofibromin (NF1) and dual specificity phosphatase 9 (DUSP9), as critical drivers of lenvatinib resistance in liver cancer. The loss of NF1 and DUSP9 can lead to the reactivation of the PI3K/AKT and MAPK/ERK signaling pathways, resulting in the inactivation of FOXO3, which in turn induces lenvatinib resistance[10]. In alignment with this, our previous report also indicated that FOXO3 is a critical mediator of sorafenib resistance in liver cancer through the autophagy signaling pathway[36]. It remains unclear whether the inhibition of HDAC *via* romidepsin affects the regulation of NF1, DUSP9 or FOXO3. However, some studies have found that the suppression of HDAC3 effectively cooperates with MAPK pathway inhibitors to target NF1-mutant melanomas[59], indicating a correlation between HDAC regulation and NF1-driven tumorigenesis. Collectively, our results suggest that restoration of normal histone acetylation status may have broad effects on rewiring lenvatinib-induced plasticity and cellular behaviors.

Recently, emerging evidence has reported that HDAC inhibitors could improve the efficacy of immunotherapy[60–63]. Treatment of romidepsin enhanced the response to anti-PD-1 immunotherapy in lung cancer by modulating T-cell chemokine expression[64]. Our results represented here that romidepsin triggered immunogenic cell death in our liver cancer r-PDCs by uplifting extracellular levels of ATP and HMGB1 and inducing phagocytosis by dendritic cell, which suggesting the role of romidepsin in leveraging immunotherapy in liver cancer and this was supported by another pan-histone deacetylase inhibitor elinostat[65]. Previously, we established human PDO co-culture models with autologous tumor-infiltrating T cells and evaluated the screened immuno-drugs *in vitro*[24,66]. In this study, we established human PDC-derived xenograft models in mice with engraftment of autologous PBMCs to examine the *in vivo* effect of romidepsin for the treatment of liver cancer with lenvatinib resistance. While the majority of T cells in PBMCs are non-tumor specific and display poor antitumor killing activity[67], incubation of these PBMCs in immuno-deficient mice would allow enough time for these non-tumor specific T cells to recognize tumor antigens expressed by human liver cells *in vivo*. We detected significant infiltration of human $CD8^+$ T cells in human PDC-derived xenograft tumor tissues, suggesting the functional human immune response *in vivo*. Consistently, we confirmed the antitumor activity of romidepsin as a single immuno-oncology agent for the treatment of liver cancer compared to sorafenib or lenvatinib. Recapitulation of human immunity in humanized mice from our approach provides reliable and powerful evaluation for the screened drugs.

5. Conclusions

In summary, the survival of patients with advanced liver cancer with clinical-lenvatinib resistance remains dismal, with novel combination treatments desperately needed. We here described a multidimensional high-throughput screening platform for the identification of effective drug susceptibility to conquer lenvatinib resistance in a clinical setting. The PDC models enable rapid screening, while the PDO and PDX models provide essential validation of screening results. The treatment of romidepsin displayed potent and durable antitumor effects in patient-derived models, both with and without the autologous immune system, by triggering immunogenic tumor cell death. The application of our multidimensional platform allows rapid discovery of drug susceptibility for advanced liver cancer with drug-resistance, thus augmenting potential personalized medicine.

Acknowledgments

This study was partly supported by the National Natural Science Foundation of China (82122069, 82073869, 30900650, 81372501, 81572260, 81773299, and H2808/82330065); Guangdong Basic and Applied Basic Research Foundation (2021B1515020004, 2020B1515120032, 2021B1212040017, and 2023B03J0106, China); the Fundamental Research Funds for the Central Universities (23yxqntd001, China); the Opening Project of Guangdong Provincial Key Laboratory of New Drug Design and Evaluation (2020B1212060034, China).

Author contributions

Guohui Wan, Zunfu Ke, Arabella H. Wan and Lei Sun conceived the idea, and wrote the manuscript; Lei Sun, Arabella H. Wan, Shijia Yan, Ruonian Liu and Zhuolong Zhou performed most experiments and analyzed data; Lei Sun, Arabella H. Wan, Ruirui Wu, Jingxing Ou and Kai Li aided in clinical sample collection; Kai Li, Xianzhang Bu, Xiongbin Lu, Zunfu Ke and Guohui Wan provided administration and supervision. All authors were involved in the final approval of the submitted and published versions.

Conflicts of interest

The authors declare no conflicts of interest.

Appendix A. Supporting information

Supporting data to this article can be found online at https://doi.org/10.1016/j.apsb.2023.09.015.

References

1. Villanueva A. Hepatocellular carcinoma. *N Engl J Med* 2019;**380**:1450–62.

2. Cordero-Espinoza L, Huch M. The balancing act of the liver: tissue regeneration *versus* fibrosis. *J Clin Invest* 2018;**128**:85−96.
3. Cancer Genome Atlas Research Network. Comprehensive and integrative genomic characterization of hepatocellular carcinoma. *Cell* 2017;**169**:1327−1341.e23.
4. Schulze K, Imbeaud S, Letouze E, Alexandrov LB, Calderaro J, Rebouissou S, et al. Exome sequencing of hepatocellular carcinomas identifies new mutational signatures and potential therapeutic targets. *Nat Genet* 2015;**47**:505−11.
5. Lee TK, Guan XY, Ma S. Cancer stem cells in hepatocellular carcinoma—from origin to clinical implications. *Nat Rev Gastroenterol Hepatol* 2022;**19**:26−44.
6. Gordan JD, Kennedy EB, Abou-Alfa GK, Beg MS, Brower ST, Gade TP, et al. Systemic therapy for advanced hepatocellular carcinoma: ASCO guideline. *J Clin Oncol* 2020;**38**:4317−45.
7. Gild ML, Bullock M, Robinson BG, Clifton-Bligh R. Multikinase inhibitors: a new option for the treatment of thyroid cancer. *Nat Rev Endocrinol* 2011;**7**:617−24.
8. Kudo M, Finn RS, Qin S, Han KH, Ikeda K, Piscaglia F, et al. Lenvatinib *versus* sorafenib in first-line treatment of patients with unresectable hepatocellular carcinoma: a randomised phase 3 non-inferiority trial. *Lancet* 2018;**391**:1163−73.
9. Jin H, Shi Y, Lv Y, Yuan S, Ramirez CFA, Lieftink C, et al. EGFR activation limits the response of liver cancer to lenvatinib. *Nature* 2021;**595**:730−4.
10. Lu Y, Shen H, Huang W, He S, Chen J, Zhang D, et al. Genome-scale CRISPR-Cas9 knockout screening in hepatocellular carcinoma with lenvatinib resistance. *Cell Death Dis* 2021;**7**:359.
11. Finn RS, Ikeda M, Zhu AX, Sung MW, Baron AD, Kudo M, et al. Phase Ib study of lenvatinib plus pembrolizumab in patients with unresectable hepatocellular carcinoma. *J Clin Oncol* 2020;**38**:2960−70.
12. Huinen ZR, Huijbers EJM, van Beijnum JR, Nowak-Sliwinska P, Griffioen AW. Anti-angiogenic agents—overcoming tumour endothelial cell anergy and improving immunotherapy outcomes. *Nat Rev Clin Oncol* 2021;**18**:527−40.
13. Adachi Y, Kamiyama H, Ichikawa K, Fukushima S, Ozawa Y, Yamaguchi S, et al. Inhibition of FGFR reactivates IFNgamma signaling in tumor cells to enhance the combined antitumor activity of lenvatinib with anti-PD-1 antibodies. *Cancer Res* 2022;**82**:292−306.
14. Torrens L, Montironi C, Puigvehi M, Mesropian A, Leslie J, Haber PK, et al. Immunomodulatory effects of lenvatinib plus anti-programmed cell death protein 1 in mice and rationale for patient enrichment in hepatocellular carcinoma. *Hepatology* 2021;**74**:2652−69.
15. Byrne AT, Alférez DG, Amant F, Annibali D, Arribas J, Biankin AV, et al. Interrogating open issues in cancer precision medicine with patient-derived xenografts. *Nat Rev Cancer* 2017;**17**:254−68.
16. Sachs N, Clevers H. Organoid cultures for the analysis of cancer phenotypes. *Curr Opin Genet Dev* 2014;**24**:68−73.
17. DiMasi JA, Reichert JM, Feldman L, Malins A. Clinical approval success rates for investigational cancer drugs. *Clin Pharmacol Ther* 2013;**94**:329−35.
18. Qiu Z, Li H, Zhang Z, Zhu Z, He S, Wang X, et al. A pharmacogenomic landscape in human liver cancers. *Cancer Cell* 2019;**36**:179−193.e11.
19. Huch M, Koo BK. Modeling mouse and human development using organoid cultures. *Development* 2015;**142**:3113−25.
20. Broutier L, Mastrogiovanni G, Verstegen MM, Francies HE, Gavarró LM, Bradshaw CR, et al. Human primary liver cancer-derived organoid cultures for disease modeling and drug screening. *Nat Med* 2017;**23**:1424−35.
21. Marsee A, Roos FJM, Verstegen MMA, Consortium HPBO, Gehart H, de Koning E, et al. Building consensus on definition and nomenclature of hepatic, pancreatic, and biliary organoids. *Cell Stem Cell* 2021;**28**:816−32.
22. Veninga V, Voest EE. Tumor organoids: opportunities and challenges to guide precision medicine. *Cancer Cell* 2021;**39**:1190−201.
23. Bose S, Clevers H, Shen X. Promises and challenges of organoid-guided precision medicine. *Med* 2021;**2**:1011−26.
24. Zhou Z, Van der Jeught K, Fang Y, Yu T, Li Y, Ao Z, et al. An organoid-based screen for epigenetic inhibitors that stimulate antigen presentation and potentiate T-cell-mediated cytotoxicity. *Nat Biomed Eng* 2021;**5**:1320−35.
25. Sun L, Wan A, Zhou Z, Chen D, Liang H, Liu C, et al. RNA-binding protein RALY reprogrammes mitochondrial metabolism *via* mediating miRNA processing in colorectal cancer. *Gut* 2021;**70**:1698−712.
26. Niu Y, Lin Z, Wan A, Sun L, Yan S, Liang H, et al. Loss-of-function genetic screening identifies aldolase A as an essential driver for liver cancer cell growth under hypoxia. *Hepatology* 2021;**74**:1461−79.
27. Crystal AS, Shaw AT, Sequist LV, Friboulet L, Niederst MJ, Lockerman EL, et al. Patient-derived models of acquired resistance can identify effective drug combinations for cancer. *Science* 2014;**346**:1480−6.
28. Deal watch. Celgene acquires Gloucester pharmaceuticals, gaining approved HDAC inhibitor. *Nat Rev Drug Discov* 2010;**9**:94.
29. Johnstone RW. Histone-deacetylase inhibitors: novel drugs for the treatment of cancer. *Nat Rev Drug Discov* 2002;**1**:287−99.
30. Bolden JE, Peart MJ, Johnstone RW. Anticancer activities of histone deacetylase inhibitors. *Nat Rev Drug Discov* 2006;**5**:769−84.
31. Galluzzi L, Senovilla L, Zitvogel L, Kroemer G. The secret ally: immunostimulation by anticancer drugs. *Nat Rev Drug Discov* 2012;**11**:215−33.
32. Furumai R, Matsuyama A, Kobashi N, Lee KH, Nishiyama M, Nakajima H, et al. FK228 (depsipeptide) as a natural prodrug that inhibits class I histone deacetylases. *Cancer Res* 2002;**62**:4916−21.
33. Yue X, Liu T, Wang X, Wu W, Wen G, Yi Y, et al. Pharmacological inhibition of BAP1 recruits HERC2 to competitively dissociate BRCA1−BARD1, suppresses DNA repair and sensitizes CRC to radiotherapy. *Acta Pharm Sin B* 2023;**13**:3382−99.
34. Li S, Chen S, Dong Z, Song X, Li X, Huang Z, et al. Concurrent silencing of TBCE and drug delivery to overcome platinum-based resistance in liver cancer. *Acta Pharm Sin B* 2023;**13**:967−81.
35. Arechederra M, Bazai SK, Abdouni A, Sequera C, Mead TJ, Richelme S, et al. ADAMTSL5 is an epigenetically activated gene underlying tumorigenesis and drug resistance in hepatocellular carcinoma. *J Hepatol* 2021;**74**:893−906.
36. Lin Z, Niu Y, Wan A, Chen D, Liang H, Chen X, et al. RNA m^6 A methylation regulates sorafenib resistance in liver cancer through FOXO3-mediated autophagy. *EMBO J* 2020;**39**:e103181.
37. Bresnahan E, Ramadori P, Heikenwalder M, Zender L, Lujambio A. Novel patient-derived preclinical models of liver cancer. *J Hepatol* 2020;**72**:239−49.
38. Neal JT, Li X, Zhu J, Giangarra V, Grzeskowiak CL, Ju J, et al. Organoid modeling of the tumor immune microenvironment. *Cell* 2018;**175**:1972−1988.e16.
39. Letai A, Bhola P, Welm AL. Functional precision oncology: testing tumors with drugs to identify vulnerabilities and novel combinations. *Cancer Cell* 2022;**40**:26−35.
40. Liu X, Krawczyk E, Suprynowicz FA, Palechor-Ceron N, Yuan H, Dakic A, et al. Conditional reprogramming and long-term expansion of normal and tumor cells from human biospecimens. *Nat Protoc* 2017;**12**:439−51.
41. Zhang Y, Huang S, Zhong W, Chen W, Yao B, Wang X. 3D organoids derived from the small intestine: an emerging tool for drug transport research. *Acta Pharm Sin B* 2021;**11**:1697−707.
42. Bayard Q, Caruso S, Couchy G, Rebouissou S, Bioulac Sage P, Balabaud C, et al. Recurrent chromosomal rearrangements of ROS1, FRK and IL6 activating JAK/STAT pathway in inflammatory hepatocellular adenomas. *Gut* 2020;**69**:1667−76.
43. Liu C, Zha Z, Zhou C, Chen Y, Xia W, Wang YN, et al. Ribonuclease 7-driven activation of ROS1 is a potential therapeutic target in hepatocellular carcinoma. *J Hepatol* 2021;**74**:907−18.
44. Noh JH, Bae HJ, Eun JW, Shen Q, Park SJ, Kim HS, et al. HDAC2 provides a critical support to malignant progression of hepatocellular

carcinoma through feedback control of mTORC1 and AKT. *Cancer Res* 2014;**74**:1728−38.
45. Lee YH, Seo D, Choi KJ, Andersen JB, Won MA, Kitade M, et al. Antitumor effects in hepatocarcinoma of isoform-selective inhibition of HDAC2. *Cancer Res* 2014;**74**:4752−61.
46. Zhang S, Jiang VC, Han G, Hao D, Lian J, Liu Y, et al. Longitudinal single-cell profiling reveals molecular heterogeneity and tumor-immune evolution in refractory mantle cell lymphoma. *Nat Commun* 2021;**12**:2877.
47. Dolly SO, Wagner AJ, Bendell JC, Kindler HL, Krug LM, Seiwert TY, et al. Phase I study of apitolisib (GDC-0980), dual phosphatidylinositol-3-kinase and mammalian target of rapamycin kinase inhibitor, in patients with advanced solid tumors. *Clin Cancer Res* 2016;**22**:2874−84.
48. Powles T, Lackner MR, Oudard S, Escudier B, Ralph C, Brown JE, et al. Randomized open-label phase II trial of apitolisib (GDC-0980), a novel inhibitor of the PI3K/mammalian target of rapamycin pathway, *versus* everolimus in patients with metastatic renal cell carcinoma. *J Clin Oncol* 2016;**34**:1660−8.
49. Chen Z, Akbay E, Mikse O, Tupper T, Cheng K, Wang Y, et al. Co-clinical trials demonstrate superiority of crizotinib to chemotherapy in ALK-rearranged non-small cell lung cancer and predict strategies to overcome resistance. *Clin Cancer Res* 2014;**20**:1204−11.
50. Izquierdo E, Carvalho DM, Mackay A, Temelso S, Boult JKR, Pericoli G, et al. DIPG harbors alterations targetable by MEK inhibitors, with acquired resistance mechanisms overcome by combinatorial inhibition. *Cancer Discov* 2022;**12**:712−29.
51. Yan B, Chen Q, Shimada K, Tang M, Li H, Gurumurthy A, et al. Histone deacetylase inhibitor targets CD123/CD47-positive cells and reverse chemoresistance phenotype in acute myeloid leukemia. *Leukemia* 2019;**33**:931−44.
52. Streubel G, Schrepfer S, Kallus H, Parnitzke U, Wulff T, Hermann F, et al. Histone deacetylase inhibitor resminostat in combination with sorafenib counteracts platelet-mediated pro-tumoral effects in hepatocellular carcinoma. *Sci Rep* 2021;**11**:9587.
53. Chang Y, Lee YB, Cho EJ, Lee JH, Yu SJ, Kim YJ, et al. CKD-5, a novel pan-histone deacetylase inhibitor, synergistically enhances the efficacy of sorafenib for hepatocellular carcinoma. *BMC Cancer* 2020;**20**:1001.
54. Roberts JL, Poklepovic A, Booth L, Dent P. The multi-kinase inhibitor lenvatinib interacts with the HDAC inhibitor entinostat to kill liver cancer cells. *Cell Signal* 2020;**70**:109573.
55. Wang X, Xu J, Sun Y, Cao S, Zeng H, Jin N, et al. Hedgehog pathway orchestrates the interplay of histone modifications and tailors combination epigenetic therapies in breast cancer. *Acta Pharm Sin B* 2023;**13**:2601−12.
56. Itoh Y, Suzuki T, Kouketsu A, Suzuki N, Maeda S, Yoshida M, et al. Design, synthesis, structure–selectivity relationship, and effect on human cancer cells of a novel series of histone deacetylase 6-selective inhibitors. *J Med Chem* 2007;**50**:5425−38.
57. Khan N, Jeffers M, Kumar S, Hackett C, Boldog F, Khramtsov N, et al. Determination of the class and isoform selectivity of small-molecule histone deacetylase inhibitors. *Biochem J* 2008;**409**:581−9.
58. Liang T, Wang F, Elhassan RM, Cheng Y, Tang X, Chen W, et al. Targeting histone deacetylases for cancer therapy: trends and challenges. *Acta Pharm Sin B* 2023;**13**:2425−63.
59. Maertens O, Kuzmickas R, Manchester HE, Emerson CE, Gavin AG, Guild CJ, et al. MAPK pathway suppression unmasks latent DNA repair defects and confers a chemical synthetic vulnerability in BRAF-, NRAS-, and NF1-mutant melanomas. *Cancer Discov* 2019;**9**:526−45.
60. Wang L, de Zoeten EF, Greene MI, Hancock WW. Immunomodulatory effects of deacetylase inhibitors: therapeutic targeting of FOXP3$^+$ regulatory T cells. *Nat Rev Drug Discov* 2009;**8**:969−81.
61. Cleophas MCP, Crişan TO, Klück V, Hoogerbrugge N, Netea-Maier RT, Dinarello CA, et al. Romidepsin suppresses monosodium urate crystal-induced cytokine production through upregulation of suppressor of cytokine signaling 1 expression. *Arthritis Res Ther* 2019;**21**:50.
62. West AC, Smyth MJ, Johnstone RW. The anticancer effects of HDAC inhibitors require the immune system. *OncoImmunology* 2014;**3**:e27414.
63. Zheng C, Zhang W, Wang J, Zhai Y, Xiong F, Cai Y, et al. Lenvatinib- and vadimezan-loaded synthetic high-density lipoprotein for combinational immunochemotherapy of metastatic triple-negative breast cancer. *Acta Pharm Sin B* 2022;**12**:3726−38.
64. Zheng H, Zhao W, Yan C, Watson CC, Massengill M, Xie M, et al. HDAC inhibitors enhance T-cell chemokine expression and augment response to PD-1 immunotherapy in lung adenocarcinoma. *Clin Cancer Res* 2016;**22**:4119−32.
65. Llopiz D, Ruiz M, Villanueva L, Iglesias T, Silva L, Egea J, et al. Enhanced anti-tumor efficacy of checkpoint inhibitors in combination with the histone deacetylase inhibitor Belinostat in a murine hepatocellular carcinoma model. *Cancer Immunol Immunother* 2019;**68**:379−93.
66. Zhou Z, Van der Jeught K, Li Y, Sharma S, Yu T, Moulana I, et al. A T cell-engaging tumor organoid platform for pancreatic cancer immunotherapy. *Adv Sci* 2023;**10**:e2300548.
67. Cafri G, Yossef R, Pasetto A, Deniger DC, Lu YC, Parkhurst M, et al. Memory T cells targeting oncogenic mutations detected in peripheral blood of epithelial cancer patients. *Nat Commun* 2019;**10**:449.